Author Manuscript

Author Manuscript

Author Manuscript

Author Manuscript

HHS Public Access

Author manuscript

Cell Rep. Author manuscript; available in PMC 2023 January 13.

Published in final edited form as:

Cell Rep. 2022 March 29; 38(13): 110582. doi:10.1016/j.celrep.2022.110582.

PRMT7 ablation stimulates anti-tumor immunity and sensitizes melanoma to immune checkpoint blockade

Nivine Srour[1,2,3,4,5], **Oscar D. Villarreal**[1,2,3,4,5,6], **Swanand Hardikar**[6], **Zhenbao Yu**[1,2,3,4,5], **Samuel Preston**[1,3], **Wilson H. Miller Jr.**[1,2,3], **Magdelena M. Szewczyk**[7], **Dalia Barsyte-Lovejoy**[7], **Han Xu**[6], **Taiping Chen**[6], **Sonia V. del Rincón**[1,2,3], **Stéphane Richard**[1,2,3,4,5,*]

[1]Segal Cancer Center, Lady Davis Institute for Medical Research, McGill University, Montréal, Québec, Canada H3T 1E2

[2]Gerald Bronfman Department of Oncology, McGill University, Montréal, Québec, Canada H3T 1E2

[3]Department of Medicine, McGill University, Montréal, Québec, Canada H3T 1E2

[4]Department of Human Genetics, McGill University, Montréal, Québec, Canada H3T 1E2

[5]Department of Biochemistry, McGill University, Montréal, Québec, Canada H3T 1E2

[6]Department of Epigenetics and Molecular Carcinogenesis, The University of Texas MD Anderson Cancer Center, Houston, TX 77030, USA

[7]Structural Genomics Consortium, University of Toronto, Toronto, Ontario, M5G 1L7, Canada

Abstract

Despite the success of immune checkpoint inhibitor (ICI) therapy for cancer, resistance and relapse are frequent. Combination therapies are expected to enhance response rates and overcome this resistance. Herein, we report that combining PRMT7 inhibition with ICI therapy induces a strong anti-tumor T cell immunity and restrains tumor growth *in vivo* by increasing immune cell infiltration. PRMT7 deficient B16.F10 melanoma exhibited increased expression of genes in the interferon pathway, antigen presentation and chemokine signaling. PRMT7-deficiency or treatment with SGC3027, a specific PRMT7 inhibitor, in B16.F10 melanoma resulted in reduced expression of DNMTs, loss of DNA methylation in the regulatory regions of endogenous retroviral elements (ERVs), and increased expression of ERVs. PRMT7-deficient cells had increased RIG-I

*Corresponding author: stephane.richard@mcgill.ca.

Author contributions

N Srour: conceptualization, data curation, formal analysis, methodology, writing—original draft and project administration; O D Villarreal: conceptualization, resources, data curation, software, formal analysis, methodology, writing—review, and editing; S Hardikar: resources, methodology; Z Yu: supervision, methodology, writing—original draft and project administration; S Preston: resources, methodology; W H Miller, Jr.: resources; M M Szewczyk: resources, methodology; D Barsyte-Lovejoy: resources, methodology, project administration, writing—review, and editing; H Xu: conceptualization, resources and data curation; T Chen: conceptualization, resources, methodology, writing; S V del Rincón: supervision, resources, methodology, project administration, and writing—original draft, review, and editing; S Richard: conceptualization, supervision, funding acquisition, project administration, and writing—original draft, review, and editing.

Competing interests

The authors declare no competing interests.

Data and software availability

The RNA-seq data is available at NCBI under accession number GSE157141.

Author Manuscript Author Manuscript Author Manuscript Author Manuscript

and MDA5 expression with a reduction in the repressive histone mark, H4R3me2s, at their promoters. Our findings identify PRMT7 as an epigenetic checkpoint for RIG-I, MDA5 and their ERV-dsRNA ligands, facilitating immune escape and anti-tumor T cell immunity to restrain tumor growth.

Keywords

PRMT7; arginine methylation; melanoma; immune checkpoint inhibitors; cytotoxic T cells; anti-tumor immunity; dsRNA; RLR pathway; DNMTs

Introduction

Arginine methylation is an epigenetic modification frequently dysregulated in cancer because of the frequent overexpression of protein arginine methyltransferases (PRMTs) (Yang and Bedford, 2013). There are three type of PRMTs, type I, II, and III, generating as final products asymmetric dimethylarginine (ADMA), symmetric dimethylarginine (SDMA) and monomethylarginine (MMA), respectively (Bedford and Clarke, 2009). High affinity specific PRMT inhibitors have been developed and are in clinical trials (Guccione and Richard, 2019). The goal is to understand which cancer patients would best benefit from these PRMT inhibitors either alone or in combination therapies (Wu et al., 2021). Links between PRMTs and immune development and function have been identified, however, the role of arginine methylation in immunotherapy is emerging (Xu and Richard, 2021).

The epigenetic modifier PRMT7 catalyzes MMA on histones (Feng et al., 2013a; Jain and Clarke, 2019; Zurita-Lopez et al., 2012) and non-histone proteins such as the eukaryotic translation initiation factor 2 alpha (eIF2α) (Haghandish et al., 2019), p38 mitogen-activated protein kinase (p38MAPK) (Jeong et al., 2020), and HSP70 (Szewczyk et al., 2020). The methylation of histone H4 by PRMT7 was shown to allosterically modulate the ability of PRMT5 to generate H4R3me2s (Feng et al., 2013a; Jain et al., 2017). PRMT7-null mice have impaired muscle (Blanc et al., 2016; Jeong et al., 2016), adipose tissue (Leem et al., 2019) and B cell germinal center formation (Ying et al., 2015). Genetic loss-of-function *PRMT7* mutations and deletions cause the SBIDDS (short stature, brachydactyly, intellectual developmental disability and seizures syndrome) syndrome (Agolini et al., 2018).

PRMTs have been involved in regulating the antiviral response (Xu and Richard, 2021). PRMT3 and PRMT7 were shown to negatively regulate the antiviral response in Zebrafish (Zhu et al., 2020a; Zhu et al., 2020b). PRMT6 was identified as an inhibitor of the TBK1 (TANK-binding kinase-1)-IRF3 (interferon regulatory factor-3) signaling cascade to attenuate the antiviral immune response (Zhang et al., 2019). PRMT5 was shown to methylate cGAS (cyclic GMP-AMP synthase), which in turn abolishes its DNA binding ability and attenuates the antiviral immune response (Kim et al., 2020; Ma et al., 2021). PRMT7 was shown to regulate the mitochondrial antiviral-signaling protein (MAVS)-mediated antiviral response (Zhu et al., 2021). Although accumulating evidence implicates PRMTs in the modulation of innate and adaptive immunity, the underlying mechanisms about how arginine methylation regulates anti-tumoral immunity is still not well understood.

Author Manuscript Author Manuscript Author Manuscript Author Manuscript

Endogenous retroviral elements (ERVs) are transposable elements (TE) derived from exogenous retroviruses that integrated into the mammalian genome. DNA hypomethylation of CpGs increases ERV expression in cancer resulting in an accumulation of double stranded RNAs (dsRNAs) (Chiappinelli et al., 2015) (Ku et al., 2021). These dsRNAs are sensed by retinoic acid-inducible gene I (RIG-I)-like receptors (RLR) signaling pathway and these triggers innate immune signaling with implications for immunotherapy (Canadas et al., 2018; Sheng et al., 2018). RLRs are RNA sensors localized in the cytosol and RIG-I (encoded by *Ddx58*) and melanoma differentiation-associated protein 5 MDA5 (encoded by *Ifih1*) are the main sensors of this pathway (Rehwinkel and Gack, 2020). Knockout studies in mice established that RIG-I and MDA5 are essential for antiviral response and type I interferon (IFN) induction in virus infection models (Kato et al., 2006).

Tumor cells evade anti-tumoral immunosurveillance and this has led to development of immune checkpoint inhibitor (ICI) therapy. The prominent mechanisms by which this occurs is the blockade of programmed death-protein 1 (PD-1) and its ligand (PD-L1) and cytotoxic T-lymphocyte-associated protein 4 (CTLA-4) and its ligands CD80 (B7.1) and CD86 (B7.2) (Wherry and Kurachi, 2015). Therapeutic approaches targeting PD-1/PD-L1 axis (Pardoll, 2012; Salmaninejad et al., 2019) and CTLA-4 have proven effective towards activating the host immune system in many cancers including melanoma (Larkin et al., 2015; Larkin et al., 2019; Topalian et al., 2016). Although immunotherapy has enhanced cancer therapy ~50% of patients fail to respond or acquire resistance to ICI therapy (Chen and Mellman, 2017; Feng et al., 2013b). The combination of ICIs and epigenetic inhibitors holds promise to fill this therapeutic gap. Inhibitors such as DNA methylation inhibitors 5-Azacytidine (5-Aza), 5-Aza-2′-deoxycytidine (5-Aza-dC; Decitabine) (Bian and Murad, 2014; Chiappinelli et al., 2015) or the histone lysine demethylase LSD1 inhibition (Sheng et al., 2018) are known to increase immune signaling (e.g. activation of IFN pathway and secretion of cytokines) and ICI therapy effectiveness. A recent study identifies H3K9 methyltransferase SETDB1 as an epigenetic checkpoint that suppresses tumor-intrinsic immunogenicity (Griffin et al., 2021).

Herein we show that depletion of the epigenetic regulator PRMT7 or its inhibition with SGC3027 in B16.F10 melanoma directly activates RLR signaling by increasing the expression of RIG-I (encoded by *Ddx58*) and MDA5 (encoded by *Ifih1*) and their ligands dsRNA-ERVs. We also report that combining PRMT7 inhibition with ICI therapy enhances anti-tumor T cell immunity.

Results

PRMT7 deficiency enhances sensitivity to anti–CTLA-4 and anti-PD-1 therapy *in vivo*

Previously, a CRISPR/Cas9 genetic screen in a murine model of melanoma (B16.F10) was performed to identify genes that, when deleted, improve anti-tumor responses to immunotherapy (Manguso et al., 2017). For this, tumor cells were injected into mice that were treated with GVAX (granulocyte macrophage colony-stimulating factor (GM-CSF)-secreting, irradiated tumor cell vaccine) alone or in combination with monoclonal PD-1 blockade to improve the immune system by stimulating anti-tumor T cell infiltration and myeloid cell activation. Interestingly, PRMT7 ranked 8th in the GVAX + PD-1 vs TCRα$^{-/-}$ CRISPR/Cas9 screen and ranked 23rd in the GVAX vs TCRα$^{-/-}$ CRISPR/Cas9 screen

Author Manuscript Author Manuscript Author Manuscript Author Manuscript

(Manguso et al., 2017). We re-analyzed their CRISPR/Cas9 screen data using our developed software called MoPAC (Gao et al., 2019), and PRMT7 remained a top hit (Supplementary Fig. S1A, S1B and Dataset S1). Moreover, we identified elevated *PRMT7* mRNA expression in skin cutaneous melanoma (SKCM) and high *PRMT7* levels were associated with reduced patient survival for melanoma (Supplementary Fig. S2A, S2B). Thus, we hypothesized that the PRMT7 epigenetic regulator promotes immunosuppression in melanoma.

To examine whether PRMT7 deficiency enhanced susceptibly to CTLA-4 and PD-1 blockade in melanoma, we generated two CRISPR/Cas9 PRMT7 depleted B16.F10 melanoma clones (sgPRMT7-1, sgPRMT7-2). The lack of PRMT7 was shown by immunoblotting and RT-qPCR (Fig. 1A, 1B) and the PRMT7 depleted cell lines displayed similar growth rates *in vitro* as control (sgCTL) cells (Supplementary Fig. S3A). We implanted sgCTL and PRMT7 depleted B16.F10 cells (sgPRMT7-1, sgPRMT7-2) subcutaneously in syngeneic C57BL6/J mice and monitored tumor growth in the absence or presence of CTLA-4 and PD-1 monoclonal antibodies (Fig. 1C-F). A combination of anti-CTLA-4 and anti-PD-1 antibodies was used to enhance the immune response (Wei et al., 2019), as PD-1 blockade alone tends to be ineffective in mice with B16.F10 tumors (Kleffel et al., 2015). Without ICI treatment, we observed a small but significant difference in tumor initiation between the sgCTL and sgPRMT7 melanoma tumors at days 3, 6 and 9, but not at the day 15 endpoint (Fig. 1C), and this effect was absence in TCR$\alpha^{-/-}$ mice (Supplementary Fig. S3B, S3C). However, treatment with the combination of CTLA-4 and PD-1 monoclonal antibodies showed a markedly reduced tumor size (> 90% at day 18) in both sgPRMT7 cell lines compared to the tumors generated by sgCTL cells and survival improved considerably (Fig. 1D). Monotherapies using anti-CTLA-4 (Fig. 1E) had a significant effect in tumor size, whereas anti-PD-1 alone (Fig. 1F) had little effect, however, monotherapies did not influence the survival.

We next tested the PRMT7 inhibitor, SGC3027, a cell active prodrug, which in cells is converted to the active compound SGC8158 (Szewczyk et al., 2020) for its ability to inhibit tumor growth. Since the prodrug is expected to have poor systemic pharmacokinetic properties, we opted for intra-tumoral delivery. B16.F10 melanoma were injected subcutaneously in C57BL/6J mice and on day 7 the mice were treated with either DMSO or SGC3027 *via* intratumoral injection (4 doses for 4 days). SGC3027-treated mice significantly decreased tumor growth and survival, as compared to mice injected with DMSO or ICI alone (Fig. 1G). Interestingly, cotreatment with SGC3027 and ICI therapy markedly improved treatment outcome and significantly reduced tumor growth and increased survival in comparison to either of the treatments alone (Fig. 1G). Taken together, these data suggest that PRMT7 depletion or inhibition renders the combined anti-CTLA-4 and anti-PD-1 treatment more efficacious at reducing tumor growth in the B16.F10 melanoma mouse model.

Loss of tumor PRMT7 expression promotes T cell infiltration and increases melanoma cell plasticity

To assess whether the difference in tumor growth observed in sgPRMT7 melanomas was due to differential immune cell infiltration into the tumors, we evaluated the immune

Author Manuscript Author Manuscript Author Manuscript Author Manuscript

composition of sgCTL and sgPRMT7-1 melanomas following anti-CTLA-4 and -PD-1 treatment. We focused on myeloid derived suppressor cell populations (MDSCs), which are known to mediate resistance in ICI therapy (Hou et al., 2020). Using multi-parameter flow cytometry (Supplementary Fig. S4), we observed a lower level of recruitment of granulocytic (G)-MDSCs and monocytic (M)-MDSCs in sgPRMT7-1 melanomas (Fig. 2A, 2B) with no difference in the frequencies of $CD3^+$ T cells or non-lymphatic dendritic cells (NLT DCs, Fig. 2C, 2D). Moreover, we observed an elevated percentage of infiltrating $CD3^+CD8^+$ T cells in tumors from mice implanted with sgPRMT7-1 treated with ICI therapy (Fig. 2E-H). Given that MDSCs accumulate in tumors and suppress T cell effector functions (Bird, 2020), together the decrease in MDSCs and the increase in $CD8^+$ T cells can play a role in reducing tumor growth of sgPRMT7 B16.F10 and could explain the markedly enhanced immune response following anti-CTLA-4 and anti-PD-1 treatment. Moreover, immunostaining using anti-cleaved caspase 3 (CCA3) and anti-Ki-67 antibodies on sgCTL and sgPRMT7-1 tumor sections show higher level of apoptosis, as an increase in CCA3 was observed with lower proliferation, as visualized by reduced Ki-67 staining in PRMT7-deficient tumors *in vivo* (Supplementary Fig. S5A, S5B).

Melanomas with high immune infiltrates have been associated with a pigmented, differentiated phenotype (Wiedemann et al., 2019). Pigmentation is regulated by MITF (microphthalmia-associated transcription factor), a determinant of melanoma cell plasticity (Du et al., 2003). Dedifferentiated melanomas, characterized by low MITF expression are generally invasive and resistant to immunotherapy (Hoek and Goding, 2010; Hoek et al., 2006). Since PRMT7 null tumors exhibited an increase in immune cell infiltration and were sensitized to immunotherapy, we postulated that PRMT7 might influence plasticity of melanoma cells (Fig. 2I-K). The sgPRMT7-1 derived tumors were indeed more pigmented, compared to sgCTL tumors (Fig. 2I). sgPRMT7-1 and sgPRMT7-2 tumors showed an increase in *MITF* mRNA and protein levels and two other melanocytic antigens GP100 (also known as Pmel17) and Melan A (also known as MART-1; Fig. 2J, 2K). These findings suggest that PRMT7 regulates melanoma cell plasticity by modulating melanocyte antigen gene expression.

PRMT7 negatively regulates the IFN-γ pathway, antigen presentation and chemokine signaling

To identify the PRMT7-mediated gene signatures that may be responsible for the increased ICI responsiveness, we performed a transcriptomic analysis of siLuc and siPRMT7 B16.F10 cells exposed or not to interferon (IFN)-γ (Fig. 3A, Supplementary Fig. S6A-C, S7, and Dataset S2). Geneset enrichment analysis (GSEA) revealed that genes related to the IFN-γ signaling pathway, antigen presentation, and chemokine signaling were significantly enriched in siPRMT7 cells (Fig. 3A, 3B and Dataset S2). Inspection of the list of genes from the RNA-seq data revealed an elevation in the IFN signaling response genes (*Trim25, Oas2, Trim21, Stat1, Nlrc5, Irf7*, and *Oas3*) in unstimulated siPRMT7 cells. Many of the IFN responsive genes regulated by PRMT7 were relevant to innate immunity and encoded key chemokines essential for recruitment of effector T cells. We also identified that several immune cell attractant chemokines (*Cxcl1, Cxcl2, Ccl2, Ccl5* and *Ccl8*) were upregulated in the RNA-seq data of the siPRMT7 cells and these were confirmed by RT-qPCR (Fig.

Author Manuscript Author Manuscript Author Manuscript Author Manuscript

3A and Fig 3C-G) and contribute to influencing the microenvironment (Li et al., 2018). Furthermore, we noted from the RNA-seq analysis that MHC-I coding genes, required for efficient display of antigens to effector T-lymphocytes (Dhatchinamoorthy et al., 2021), were upregulated in siPRMT7 cells (Fig. 3H). Known regulators of MHC class I genes, *Nlrc5* (nucleotide-binding oligomerization domainlike receptor family caspase recruitment domain containing 5) (Kobayashi and van den Elsen, 2012) and its target genes *Psmb9* (proteasome 20s subunit beta 9), *B2m* (Beta-2 microglobulin) and *Tap1* (antigen peptide transporter 1) were also elevated in siPRMT7 or SGC3027 treated B16 cells (Fig. 3I, 3J). These increases could be responsible to drive T cell responses against PRMT7 depleted tumors. Similar increases were observed in human melanoma A375 and SK-Mel-28 cell lines (Supplementary Fig. S8A, S8B). Interestingly, treatment of B16 cells with the PRMT5 inhibitor (EPZ015666) also showed a significant increase in all MHC class I related genes (Fig. 3J), as described previously (Kim et al., 2020). A similar trend was observed with MS023 (PRMT1 inhibitor), except for *Psmb9* (Fig. 3J). In contrast, the CARM1 inhibitor (TP064) decreased *Nlrc5* expression, and increased *Tap1* mRNA levels, but did not affect *Psmb9* and *B2m* expression levels. These finding suggest that PRMT7 negatively regulates MHC-I gene expression, which then limits antigen presentation and enhances tumor evasion.

PRMT7 epigenetically suppresses antitumoral immunity by inhibiting RLR pathway

Gene Ontology (GO) enrichment analysis of the differentially expressed genes between siLuc and siPRMT7 B16.F10 melanoma cells revealed top categories including innate immune response, and defense response to viruses (Supplementary Fig. S9). To further investigate the function of PRMT7 in innate responses, we first considered that PRMT7 might trigger cytosolic sensors (Rehwinkel and Gack, 2020). For this, we examined whether PRMT7 regulated the RLR pathway. Notably, PRMT7 deficiency increased the protein level of RIG-I (encoded by *Ddx58*) and MDA5 (encoded by *Ifih1*) (Fig. 4A). RIG-I and MDA5 protein levels increased in sgPRMT7 cells after transfection with poly (I:C), ligands for RIG-I and MDA5, used to mimics of viral infection (viral mimicry) or dsRNA sensing (Fig. 4A). Also, we found that PRMT7 deficiency promoted the activation and phosphorylation of IRF3 (p-IRF3) (Fig. 4A). IRF3 is a key transcription factor for IFN-β gene expression (Yanai et al., 2018). Next, we examined the effects of PRMT7 deletion on IRF3 activation. Our data show an increase induction of *Ifn-β* mRNA level (Fig. 4B) and other proinflammatory cytokines (*Il-6, Cxcl9* and *Cxc10*) (Fig. 4C-E). Taken together, these data indicate that PRMT7 acts as a suppressor of the RLR pathway and regulates both RIG-I and MDA5-induced immunity. To further confirm the regulatory roles of PRMT7 in RLR, we performed knockdown of the main innate immune sensors: RIG-I and MDA5 using siRNA. Strikingly, siRNA-targeting RIG-I and MDA5 repressed the effect of PRMT7 deletion on interferon genes (IFNs: *Ifn-α*, *Ifn-β,* and *Il-28*) and on a panel of IFN-stimulated genes (ISGs: *Oasl* and *Isg15*) by at least two-fold (Fig. 4F), suggesting that PRMT7 regulates IFN gene expression *via* RIG-I and MDA5.

PRMT7 regulates *Ddx58* and *Ifih1* expression by regulating H4R3me2s at their promoters

To identify epigenetic targets of PRMT7, we performed chromatin immunoprecipitation (ChIP) assays to test whether PRMT7 is localized at the *Ddx58* or *Ifih1* in B16.F10 cells. ChIP analysis showed that PRMT7 bound to the promoter regions of both *Ddx58* and

Author Manuscript Author Manuscript Author Manuscript Author Manuscript

Ifih1 (Fig. 4G). Though established that PRMT7 can only form MMA, it has been shown to modulate the levels of H4R3me2s *in vivo* (Feng et al., 2013a). Thus, we proceeded to examine for the presence of H4R3me2s at the *Ddx58* and *Ifih1* promoter regions by ChIP analysis. Indeed, we detected a dramatic decrease in H4R3me2s in PRMT7-depleted B16.F10 cells (Fig. 4H and Supplementary Fig. S10A). Due to the ability of PRMT7 to influence neighboring histone marks, we assessed the presence of H3K4me3 (a hallmark of gene activation) at the the *Ddx58* and *Ifih1* promoters. ChIP assay showed that H3K4me3 was increased at both *Ddx58* and *Ifih1* promoter regions when PRMT7 was deleted (Fig. 4I and Supplementary Fig. S10B). We also performed ChIP on *Ddx58* and *Ifih1* promoter regions for other histone arginine marks including H3R2me2s and H3R8me2s, as controls, and our data showed no significant difference in these histone marks between sgCTL and sgPRMT7 cells (Supplementary Fig. S10C, S10D). Using acid extraction, we monitored total histone arginine methylation marks by immunoblotting, and we observed that only H4R3me2s level was decreased in sgPRMT7 B16.F10 cells (Fig. 4J) and in B16.F10 cells transfected with siPRMT7 (Supplementary Fig. S10E). These findings suggest the *Ddx58* and *Ifih1* transcriptional levels are increased due to the reduced levels of H4R3me2s influenced by PRMT7. Our findings identify PRMT7 as an epigenetic regulator of RLR pathway by directly targeting RIG-I and MDA5.

Deletion of PRMT7 induces ‘viral mimicry’ through ERVs, dsRNA, and stress granules (SGs) formation

RLR activation pathway observed in sgPRMT7 cells leads to enhanced antitumor activity through IFN production. This led us to hypothesize that IFN activation might be the result of dsRNA generation from ERVs. Furthermore, many reports have linked ERVs to the activation of innate immune functions *via* IFN transcription and the regulation of tumor responses to host immunity (Chiappinelli et al., 2015; Kassiotis and Stoye, 2016; Roulois et al., 2015). To explore this possibility, we first measured the levels of ERVs and IFN genes by RT-qPCR in sgCTL and both sgPRMT7-1 and sgPRMT7-2 B16.F10 melanoma cells. We observed that PRMT7 deletion increased ERV transcripts (*MuERV-L, IAP, MusD,* and *Line-1*), IFN genes (*Ifn-α, Ifn-β* and *Il-28*), and IFN-stimulated genes (ISGs) (*Oasl, Isg15, Rig-1/Ddx58* and *Ifit,* Fig. 5A). Similar increase in ERVs and IFN genes was also observed in human melanoma A375 and SK-Mel-28 cell lines (Supplementary Fig. S11A, S11B).

We next examined whether bidirectional transcription producing sense and antisense transcripts of the murine subtype of ERVs: *MuERV-L* (Benit et al., 1997) and *IAP (intracisternal A-particles)* (Qin et al., 2010) could be detected using the TAG-aided sense and antisense transcript detection (TASA-TD) assay (Henke et al., 2015). Indeed, we detected higher levels of sense and antisense transcripts for *MuERV-L* and *IAP* in sgPRMT7 compared to sgCTL cells, but not *β-actin*, used as negative control (Fig. 5B), suggesting a role for PRMT7 in transcriptionally silencing ERVs. Such bidirectional expression is known to generate dsRNAs (Su et al., 2012) that trigger IFN responses (Berrens et al., 2017; Gantier and Williams, 2007; Okamura and Lai, 2008). To monitor if the loss of PRMT7 caused the dsRNA accumulation, we treated total RNA from sgCTL, sgPRMT7-1 and sg-PRMT7-2 B16.F10 cells with RNase A, under high salt condition to cleave single stranded (ss)RNAs and preserve the dsRNAs. Indeed, RT-qPCR data showed dsRNA enrichment

Author Manuscript Author Manuscript Author Manuscript Author Manuscript

for a number of ERVs and other retrotransposons (*MuERV-L, IAP, MusD,* and *Line-1*) in sgPRMT7 cells compared to sgCTL under these conditions (Fig. 5C). Moreover, the dsRNA specific anti-J2 antibody detected dsRNAs in an RNase III-dependent manner by RNA dot blot and the presence of intracellular dsRNAs in sgPRMT7 cells was higher than in sgCTL cells (compare dots 1 and 2, Fig. 5D, 5E). Our findings show an accumulation of dsRNAs in the absence of PRMT7.

Sensing of the dsRNA, implicated in the innate immune response, was shown to be facilitated by stress granules (SGs) formation (Burgess and Mohr, 2018). The later have antiviral activity and can mediate innate immunity through the SG nucleation component G3BP1 (DeWitte-Orr et al., 2009; McCormick and Khaperskyy, 2017). Thus, we investigated whether sgPRMT7 cells had increased G3BP1-positive SGs. Indeed, sgPRMT7 cells had increased number of SGs after sodium arsenite or 45°C heat shock treatment (Fig. 5F, 5G). Given that the dsRNA-dependent protein kinase PKR is considered to play a role in IFN response to viral infection (Balachandran et al., 2000), we wanted to investigate whether the phenotype we observed in sgPRMT7 cells, linked to SGs formation, was PKR dependent. To test this hypothesis, we performed a PKR knockdown in sgCTL and sgPRMT7 cells and assessed the phosphorylation of eukaryotic initiation factor-2 (p-eIF2) by immunoblotting (Fig. 5H). An increase in p-eIf2α in sgPRMT7 cells was observed. This effect was abolished with PKR-depletion, indicating that SGs formation in sgPRMT7 cells was dependent on PKR-eIf2α axis. The phosphorylation of eIf2α in sgPRMT7 was followed by an increase in eIf2α target genes (*Atf4, Bip* and *Xbp1*) (Fig. 5I). These observations are in agreement with the finding that SG formation can function as a platform for the recognition of viral RNAs by activating RLR signaling pathway (Ng et al., 2013). Taken together, our findings show that loss of PRMT7 in B16.F10 cells induces a “viral mimicry” response with elevated ERVs and an increase in SG formation leading to RLR activation and type-I IFN induction.

sgPRMT7 B16 cells have reduced DNMT1, DNMT3a, and DNMT3b expression

DNMT inhibitors are known to upregulate immune signaling through inducing ERVs in primary tumors, thus enhancing the sensitivity of tumors to immunotherapy (Chiappinelli et al., 2015; Zhang et al., 2017). As PRMT7 is known to influence DNA methylation (Jelinic et al., 2006), we wanted to investigate whether PRMT7 affected the expression of DNMTs in B16.F10 melanoma cells. Our transcriptomic analysis (RNA-seq) showed an ~2-fold reduction in the expression of *Dnmt1* and a slight decrease in *Dnmt3a* and *Dnmt3b* expression (Dataset S1). RT-qPCR in sgCTL and sgPRMT7 B16 cells confirmed the reduced expression of *Dnmt1*, *3a* and *3b* mRNAs in sgPRMT7 cells (Fig. 6A). Moreover, the protein levels of DNMT1, 3a and 3b were also reduced in both sgPRMT7-1 and sgPRMT-2 compared to sgCTL cells (Fig. 6B). Hypomethylating agents are known to activate innate immunity (Roulois et al., 2015), influence T-cell priming, modulate immune suppressive cells (Kim et al., 2014) and sensitize to ICI therapy through induction of ERVs in a pre-clinical model of melanoma (Chiappinelli et al., 2015). We tested the effect of 5-Aza in our model, and we observed that sgPRMT7 cells increased ERV expression to a similar level as 5-Aza treated sgCTL cells (Fig. 6C). Notably, 5-Aza treated sgPRMT7 cells did not have a further increase in ERV expression, indicating that PRMT7 and 5-Aza likely

Author Manuscript Author Manuscript Author Manuscript Author Manuscript

converge in the same pathway. We next examined whether PRMT7 influenced ERVs *via* the expression of the DNMTs. To explore this hypothesis, we asked whether PRMT7 deletion would affect DNA methylation in the 5' long terminal repeats (5' LTRs) of *MuERV-L, IAP* and *MusD* and the 5' untranslated region (5' UTR) of *Line-1*. Bisulfite sequencing analysis showed that, compared to sgCTR-treated cells, PRMT7 depletion resulted in losses of DNA methylation by >20% at all the loci examined, similar to the effects of 5-Aza treatment (Fig. 6D). Our findings suggest that DNA hypomethylation at ERV loci is responsible for their expression.

Clinical relevance of PRMT7 expression in response to ICI therapy in human melanoma patients

To assess the clinical significance of our findings, we analyzed whether *PRMT7* mRNA expression could be used as a predictor of ICI response. Due to lack of studies on human melanoma patients before and after ICI treatment, we took advantage from RNA-seq data of two cohorts of melanoma patients treated with anti-PD-1 therapy and we re-analyzed them (Hugo et al., 2016; Riaz et al., 2017). Transcriptomic database of 28 patients treated with anti-PD-1 therapy showed that patients presenting a complete response to ICI treatment had the lowest mRNA level of *PRMT7* at pre-treatment (Hugo et al., 2016), suggesting that low *PRMT7* expression might predict a better ICI outcome (Fig. 7A, 7B). The same analysis was performed for a melanoma cohort treated with Nivolumab (anti-PD-1) (Riaz et al., 2017) and the data showed that low *PRMT7* expression level was partially correlated with a better response to ICI (Fig. 7C, D). The patients with a complete response (CR) showed the lowest level of *PRMT7* in pre-treatment biopsy and 29 days after the immunotherapy treatment, compared to other groups (PR: Poor Response; SD: Stable Disease; and PD: Progressive Disease). Interestingly *PRMT7* gene expression was more pronounced in patients with poor responses (Fig. 7C, 7D).

In addition, we performed CD3 immunohistochemical (IHC) staining on formalin-fixed paraffin-embedded (FFPE) patient derived melanoma samples treated with anti-PD-1 plus carbotaxol (n=9) to establish an immune score. Our data showed that patients who responded better to ICI (GR: Good Responders) presented a higher immune score (2-moderate, 3-severe), compared to PR patients presenting a weak immune score (1-focal) (Table 1). These findings suggest a positive correlation between $CD3^+$ T cells (immune infiltration) with the ICI outcome. Moreover, we performed PRMT7 IHC staining on same FFPE patient derived melanoma samples and found that in patients exhibiting a poor response (PR) to ICI therapy, 50% of melanomas stained positively for PRMT7 (Table 1). In contrast, in patients that were GR to ICI, their melanomas had a higher immune score (2-moderate, 3-severe) than PR, and only 20% of melanomas stained positive for PRMT7. In addition, we showed that the expression of PRMT7 in human cancers negatively correlated with T cell cytotoxicity markers in TCGA datasets using TIMER (Tumor Immune Estimation Resource) method (Li et al., 2017). We observed that lower expression of *PRMT7* is partially correlated with higher cytotoxic activity contributed mainly by $CD8^+$ T cells and granzyme B (GZMB) in skin cutaneous melanoma (SKCM) (Supplementary Fig. S13A, S13B). Also, we highlighted a global negative "partial" correlation between PRMT7 expression and the abundance of subsets of immune infiltration cells including B

Author Manuscript Author Manuscript Author Manuscript Author Manuscript

cells, $CD8^+$ T cells, macrophages, neutrophils, and dendritic cells in SKCM (Supplementary Fig. S13C), suggesting an important role for PRMT7 in reformatting the tumor immune microenvironment in melanoma. Taken together, our findings show a trend towards a correlation between PRMT7 expression, immune infiltration, and clinical response.

Discussion

In the present manuscript, we identify PRMT7 as a regulator of immunotherapy sensitivity for melanoma B16.F10 cells. CRISPR/Cas9 deletion of PRMT7 (sgPRMT) in B16.F10 cells resulted in enhanced anti-tumoral immunity following anti-CTLA-4 and PD-1 treatment and smaller tumor formation when injected subcutaneously in syngeneic mice. The small tumors observed with sgPRMT7 treated with ICIs had increased infiltration of $CD8^+$ T cells with a decrease in G-MDSCs and M-MDSCs *in vivo.* Moreover, the sgPRMT7 generated melanomas had increased pigmentation associated with a melanocytic differentiated phenotype. Transcriptomic analysis by RNA-seq showed that PRMT7 is a regulator of gene expression for the IFN pathway, antigen presentation, and chemokine signaling through the regulation of RLR pathway. Mechanistically, we show that PRMT7-deficiency lowered the expression of DNMT1, DNMT3a, and DNMT3b with hypomethylation of ERV loci and increasing dsRNA ERV expression. PRMT7 inhibition also increased the expression of RIG-I and MDA-5 by regulating the presence of histone marks (H4R3me2s and H3K4me3) on their promoters. Finally, we show an inverse correlation between PRMT7 expression and ICI response in melanoma patients. These findings suggest that therapeutically inhibiting PRMT7 markedly improved ICI treatment outcomes in melanoma model (Fig. 8, see model).

We showed that sgPRMT7 tumors were less responsive to monotherapies alone (anti-CTLA-4 or anti-PD-1). CTLA-4 and PD-1 have different cellular and molecular mechanisms regarding T cell activation with the main difference being that anti–CTLA-4, but not anti–PD-1, expands CD4 effector T cells (Pardoll, 2012; Wei et al., 2019). Thus, the dual blockade using anti-CTLA-4 and anti-PD-1 antibodies would manifest as distinct effects on antitumor T cell populations compared with monotherapies, resulting in a superior tumor eradication. Our data demonstrate a synergy between PRMT7 inhibition and ICIs in controlling melanoma tumor growth. Interestingly, the combination of ICI and PRMT7 deficiency was stronger when the pharmacological inhibitor of PRMT7 (SGC3027) was administered in the tumor compared to deletion of PRMT7 in the tumor genetically by CRISPR/Cas9 (i.e. sgPRMT7). These data suggest that inhibiting PRMT7 in the tumor microenvironment further contributes to enhancing tumor immunity. These findings address an unmet clinical need, namely, the ability to combine PRMT7 inhibition and ICI therapy in “cold” tumors, which are not responsive to ICI therapy.

Epigenetic regulation such as histone acetylation (Hogg et al., 2017; Woods et al., 2015) and histone methylation (Lu et al., 2017; Toyokawa et al., 2019) plays a crucial role in regulating response to ICIs. Our findings that PRMT7 is an epigenetic regulator of RIG-I and MDA5 expression through regulating the level of H4R3me2s at their promoters provide a new therapeutic mechanism for the control of RLR signaling pathway and innate antitumoral immunity stimulating IFN and cytokine production. PRMT7-mediated

Author Manuscript Author Manuscript Author Manuscript Author Manuscript

H4R3me2s decrease at *DNMT3b* and *CDKN1a* promoters has been observed in muscle stem cells (Blanc et al., 2016). PRMT7 also influences the methylation of H4R3 levels at the *BCL6* gene and negatively regulates its expression for germinal center formation and plasma cell differentiation (Ying et al., 2015). The H3K4me3 increase at the *Ddx58/Ifih1* promoters is consistent with PRMT7 regulation of mixed-lineage leukemia 4 (MLL4) catalyzed H3K4me3 level (Dhar et al., 2012).

Our data showed an elevated infiltration of $CD8^+$ T cells and a decreased presence of G-MDSCs and M-MDSCs in sgPRMT7 melanomas *in vivo.* High levels of G-MDSCs and M-MDSCs are known to promote an immunosuppressive environment in skin cancer (Fujimura et al., 2012). Furthermore, we showed that PRMT7 deletion increases IFN-γ signaling pathways. IFN-γ is known to enhance cytotoxic T lymphocyte (CTL) function (Bhat et al., 2017) and inhibit MDSCs function (Medina-Echeverz et al., 2014). A robust IFN-γ response in NSCLC patients and melanoma patients treated with ICIs is accompanied with a significantly longer progression-free survival (Higgs et al., 2018). Tumor cell loss of the *IFNGR1* gene results in resistance to anti-PD-1 (Shin et al., 2017) and anti-CTLA-4 therapies (Gao et al., 2016).

PRMT7 is known to allosterically influence the PRMT5-catalyzed H4R3me2s (Jain et al., 2017). As H4R3me2s decreases on *Ddx58* and *Ifih1* promoters it is likely that in PRMT7-deficient B16.F10 melanoma this is indirectly mediated by PRMT5. Consistent with this possibility is the fact that melanoma deficient for PRMT5 upregulate the IFN pathways, MHC-I related genes (*Nlr5, B2m, Bsmp9, Tap1*), and chemokine production (Kim et al., 2020; Ma et al., 2021). Thus, we provide an epigenetic role for PRMT7 in the regulation of the RLR signaling pathway by directly targeting the transcriptional regulation of *Ddx58* and *Ifih1* promoters.

DNMT inhibitors increase the expression of ERVs in cancer and this activates the innate antiviral response (Chiappinelli et al., 2015). We found that the loss of PRMT7 suppressed DNMT expression at the mRNA and protein levels by a hitherto undetermined mechanism. PRMT7 loss in melanoma triggered dsRNA-ERVs as the result of DNA hypomethylation at ERV loci. It is known that PRMT7 influences the expression of DNMT3b in muscle stem cells (Blanc et al., 2016) and PRMT7 is known to regulate DNA imprinting (Jelinic et al., 2006). Crosstalk between histone modifications and DNA methylation is known to occur (Esteve et al., 2006; Lehnertz et al., 2003; Vire et al., 2006; Wu et al., 2021). ERVs are generally repressed by DNA methylation. Treatment with DNMT inhibitors induces demethylation at ERV loci and stimulates viral defense signaling in human embryonic stem cells by increasing their expression (Maksakova et al., 2008). Our results show that PRMT7 loss, by downregulating DNMTs, likely leads to ERV hypomethylation associated with increased dsRNA-ERVs. The type I IFN is indeed mediated by dsRNA-ERVs as this induction was repressed with siRIG-I and siMDA-5 in sgPRMT7 cells. Thus, we identify PRMT7 as a potent regulator of ERV expression and signaling.

In conclusion, our findings show that PRMT7 inhibition elicits anti-tumor immunity associated with increase immunogenicity and T cell infiltration. Our data provide the impetus for further drug development for more effective PRMT7 inhibitors (Szewczyk et

Author Manuscript Author Manuscript Author Manuscript Author Manuscript

al., 2020), as these can potentially be combined with immune-based therapies to achieve synergy. Future studies will be directed at ascertaining the use of PRMT7 inhibition across different cancer types and to examine if PRMT7 could be used as a biomarker for ICI responsiveness.

Materials and Methods

In vivo CRISPR screening analysis in B16.F10 tumor cells

The differential analysis of the CRISPR screen performed by Manguso et al. (Manguso et al., 2017) was carried out with the MoPAC v3.1 (Modular Pipeline for Analysis of CRISPR screens) R package (Gao et al., 2019). In brief, the log-fold-change at both the sgRNA and gene levels were first obtained from the table of read counts with a quality control module. Afterwards, a normalization module was used to compute unbiased measures of sgRNA and gene essentiality. The statistical significance was assessed based on: (1) the Z-score of the differential gene essentiality, (2) Student's *t*-test applied to the biological replicates of gene essentiality and (3) a novel bidirectional version of MAGeCK's αRRA algorithm (Li et al., 2014)applied to the differential sgRNA essentiality. The MoPAC tool is publicly available at https://sourceforge.net/projects/mopac/.

Generation of sgPRMT7 B16.F10 cells

The B16.F10 melanoma cell line was kindly provided by Dr. Michael Pollak (McGill University). These cells were subjected to CRISPR/Cas9-Mediated knockout of PRMT7 by transient co-transfection of the Cas-9 single guide RNA (sgRNA)-GFP plasmid (Addgene #Px458) and the PRMT7 sgRNA plasmid (IDT: #270436658), targeting the exon four with the following gRNA sequence: 5'-*AAA ATA CTA CCA GGG TAT CCG GG*-3'. $5x10^5$ cells were plated in a six-well plate and were co-transfected the following day using 2μg of pX459 (Cas-9) plasmid DNA and 2μg of PRMT7 sgRNA plasmid DNA using Lipofectamine 3000 (Invitrogen) according to manufacturer's instruction. 24 hours later, GFP positive cells were isolated using FACS-ARIA sorter (Beckton Dickinson). After selection, cells were grown for 14 days *in vitro* before being tested for the deletion of PRMT7 by immunoblotting and subsequently the deletion junction sequenced by Sanger DNA Sequencing. Two positive clones (sgPRMT7-1, sgPRMT7-2) and one negative clone (sgCTL) were selected to be used for the experiments.

Cell lines

B16.F10 murine melanoma cell lines, A375 and SK-Mel-28 human cell lines were maintained in Dulbecco's modifies Eagle's medium (HyClone), supplemented with 10% Fetal Bovine Serum (FBS: HyClone), 1% penicillin/streptomycin (Multicell) and 1% sodium pyruvate (Multicell) in a 5% CO_2 incubator at 37 °C.

Animals

All mouse procedures were performed in accordance with McGill University guidelines, which are set by the Canadian Council on Animal Care. Seven to twelve-week-old wild type female C57BL/6J mice were obtained from Jackson laboratories (Stock No: 000664). A colony of B6.129S2-Tcra^{tm1Mom}/J (Tcra$^{-/-}$) T cell-deficient mice were also obtained from

Author Manuscript Author Manuscript Author Manuscript Author Manuscript

Jackson laboratories (Stock No: 002116). Mice were age-matched to be 7 to 12 weeks old at the time of tumor inoculation. Mice were subcutaneously injected with $1x10^6$ cells/100μl into the right flank on day 0. On day 3, 6, 9 and 12, mice were treated with 100μl of monoclonal anti-PD-1 (anti-mouse CD279, clone: RMP1-14, Cat #BE0146, *In Vivo*MAb) and 100μl of anti-CTLA-4 (anti-mouse CD152, clone: 9H10, Cat #BE0131, *In Vivo*MAb) *via* intraperitoneal injection. Tumors were measured every two to three days beginning on day 3 after challenge until the time of sacrifice. Measurements were taken manually with a caliper by collecting the longest dimension (length) and the longest perpendicular dimension (width). We estimated the tumor volume with the formula: $(L\times W^2)/2$. CO_2 inhalation was used to euthanize mice 15 days after tumor inoculation for tumor collection. For the PRMT7 inhibitor injection *in vivo*: 7 to 12 weeks old mice were subcutaneously injected with $1x10^6$ cells/100μl B16.F10 melanoma cells into the right flank on day 0 and then intratumorally injected with 10 μM of DMSO or SGC3027 (PRMT7 inhibitor) on day 7, 8, 9 and 10 with or without intraperitoneal injection with anti-PD-1 and anti-CTLA-4 on day 3, 6, 9 and 12. Tumor size and overall survival were measured and calculated as described above.

Cell culture, transfections and treatments

Melanoma cell lines were seeded into six-well plates on day 1, targeting 70–80% of confluence on the day of analysis. On day 2 after siRNA transfection, cells were exposed to 100 IU/ml interferon gamma (MACS Miltenyi Biotec #130-105-785) for 24 hours. For poly (I:C) treatment: sgCTL and sgPRMT7 B16.F10 melanoma cells were transfected with poly (I:C) LMW (Low Molecular Weight) (InvivoGen, Cat #31852-29-6) at 2.5 μg/ml using Lipofectamine 3000 (Invitrogen) for 24 hours. Whole cells were then collected for further analysis (RT-qPCR or Western blot). For siRNA and vector transfections, B16.F10 cells were transfected using Lipofectamine RNAiMAX (Invitrogen) and Lipofectamine 3000 (Invitrogen) respectively, according to the manufacturer's instruction. All siRNAs (20 to 40 nM) were purchased from Dharmacon and the sequences are as follow: siPRMT7 (siGenome SMARTpool mouse PRMT7#214572 siRNA, Catalog ID: M-053294); *siPRMT7#1: 5' -GGA CAG AAG GCC UUG GUU C- 3'; siPRMT7#2: 5' -GAG CGG AGC AGG UGU UUA C- 3'; siPRMT7#3: 5' -UCA GCU AUG UUG UGG AGU U- 3'; siPRMT7#4: 5' -GUA GCU UCC UAU AGA CUG A- 3'*; siPRMT5 (siGenome SMARTpool mouse PRMT5#27374 siRNA, Catalog ID: M-042281); *siPRMT5#1: 5' -CAA CCG AGA UCC UAU GAU U- 3'; siPRMT5#2: 5' -GGA AUA CGC UAA UUG UGG G- 3'; siPRMT5#3: 5' -GUC CGU GCC UGU CGG GAA A - 3'; siPRMT5#4: 5' -CAG UUU AUC AUC ACG GGA A- 3'*. siDDX58/RIG-I (siGenome SMARTpool mouse DDX58#230073 siRNA, Catalog ID: M-065328); *siDDX58#1: 5' - UGG AAC AGG UCG UUU AUA A - 3'; siDDX58#2: 5' - GAC AGA CGC UCU AAA UUA C - 3'; siDDX58#3: 5' - GUU AGA GGA ACA CAG AUU A - 3'; siDDX58#4: 5' - GUA CAA CAU UGC GAG CAU U - 3'*; siMDA5/IFIH1 (siGenome SMARTpool mouse IFIH1#71586 siRNA, Catalog ID: M-048303); *siIFIH1#1: 5' - GAA CGU AGA CGA CAU AUU A - 3'; siIFIH1#2: 5' - ACA CGA UAC UGG AAC AAU U - 3'; siIFIH1#3: 5' - GUU AUG GCC UUG UCA CGA A - 3'; siIFIH1: 5' - GGU AUC GAA UUA UUG GAU U - 3'* and siEif2ak2/PKR (siGenome SMARTpool mouse Eif2ak2#s19106 siRNA, Catalog ID: M-040807); *siEif2ak2#1: 5' – GGA AAG AGA UAC GCU AUU A - 3'; siEif2ak2#2: 5' – CAA AUG GAA UUC UGU GAU A - 3'; siEif2ak2#3: 5' – CGA CUU CUC UAA UGA*

Author Manuscript Author Manuscript Author Manuscript Author Manuscript

UAU A - 3'; siEif2ak2#4: 5' – GAA AUU GGC UUA GGU GGA U - 3'. The *siRNA 5'-CGU ACG CGG AAU ACU UCG AdTdT-3'*, targeting the firefly luciferase (GL2) was used as control (siLuc).

RT-qPCR

Total RNA from cells were isolated with TRIzol (Invitrogen) according to manufacturer's instruction. After digestion with DNase I (Promega), 1 μg of total RNA was converted to cDNAs using M-MLV reverse transcriptase (Promega). Real-time quantitative PCRs were performed using PowerUp SYBR Mastermix (Life Technologies #A25742) on 7500 Fast Real-Time PCR System (Applied Biosystem). Results were normalized as described in the figure legends using the ΔΔct method. Primers used in this study are outlined in Dataset S3.

Protein extracts and immunoblot analysis

Whole lysates from B16.F10 melanoma cells were prepared in 2x Laemmli buffer and boiled at 100°C. Equal amounts of protein samples were loaded, separated on 10% SDS-PAGE gels, transferred to nitrocellulose membranes using an immunoblot TurboTransfer system (Bio-Rad) and probed with corresponding antibodies listed in Dataset S3. Immunoblot signals were detected using chemiluminescence (Perkin Elmer).

Histone acid extraction

B16.F10 cells were harvested at a cell density of 10^7 cells per ml and washed twice with ice-cold PBS. Cells were then resuspended in Triton Extraction Buffer (TEB) containing 0.5% Triton X 100 (v/v), 2 mM phenylmethylsulfonyl fluoride (PMSF) and 0.02% (w/v) NaN3. Cells were then lysed on ice for 10 min with gentle stirring followed by spinning at 6,500 x g for 10 min at 4°C to spin down the nuclei. The nuclei were then washed in half the volume of TEB and centrifuge as before. The pellet was resuspended in 0.2 N HCl and the histones were extracted over night at 4°C. Samples were then centrifuge at 6,500 x g for 10 min at 4°C to pellet debris and the supernatant was incubated with 2M NaOH at 1/10 of the volume of the supernatant to neutralise HCl. Equal amount of histone samples was then dissolved in 2× Laemmli buffer and separated on 15% Tris-HCl gels. The Abs used for western blots are listed in Dataset S3.

Flow cytometry analysis

B16.F10 cells were transfected with the corresponding siRNA and then treated or not with 100IU/mM interferon gamma (Mouse IFN-γ, Cat#130-105-785, MACS, Miltenyibiotec) for 24 hours. On day 3, cells were blocked with Fc-Block and thein stained with anti-PD-L1 antibody (CD274-clone: #558091, BD-Pharmingen). For immune cell composition analysis: Primary tumors were collected on day 15, weighed, mechanically diced, incubated with collagenase P (2 mg/ml, Sigma-Aldrich) and DNase I (50 μg/ml, Sigma-Aldrich) for 10 min, and pipetted into a single-cell suspension. Cells were then blocked with anti-mouse CD16/32 antibody (BioLegend) and stained with indicated antibodies (Dataset S3) as well as a Live/Dead discrimination dye (BD Biosciences). Data were subsequently acquired at the LSR Fortessa flow cytometer and results were analyzed using FlowJo software.

Author Manuscript Author Manuscript Author Manuscript Author Manuscript

Immunofluorescence (IF)

B16.F10 tumors were fixed for 24 hours in 10% neutral-buffered formalin and then permeabilized in 70% ethanol overnight. Briefly, tissue sections were blocked in 10% normal goat serum in PBS with 0.3% Triton X-100/PBS solution for 1 hour, followed by primary antibody incubation overnight at 4°C. For G3BP1 staining, B16 cells were growing on glass coverslips and treated with 0.5 mM sodium arsenite (NaAS2O3, Sigma S1400) for 1 h or heat shock at 45°C for 30 min. Cells were then fixed for 10 min with 4% paraformaldehyde (PFA), washed with PBS and permeabilized for 5 min with 0.25% Triton X-100 in PBS. Coverslips were then incubated with blocking buffer containing 5% FBS for 1h, and incubated with G3BP1 antibodies for 2h at RT. After three washes, slides and coverslips were incubated with corresponding fluorescent secondary antibodies for 1 hour at RT and mounted with IMMUMOUNT (Thermo Scientific) mounting medium containing 1μg/ml of 4′,6-diamidino-2-phenylindole (DAPI). Images were taken using a Zeiss M1 fluorescence microscope and analyzed by ImageJ.

Immunohistochemical Staining (IHC) and scoring

Human melanoma patient samples were obtained from the Sir Mortimer B Davis Jewish General Hospital, Montreal, Quebec, Canada. Patients with melanoma were treated with a combination of anti-PD-1 and carbotaxol and pre-treatment tumor tissues were obtained for IHC staining performed on a Ventana Discovery Benchmark XT. Briefly, formalin-fixed, paraffin-embedded tumor sections were stained with CD3 (Ventana Benchmark: clone 2GV6 at 1:50) (Taube et al., 2014) and PRMT7 (Sigma #HPA044241 at 1:10) antibodies, followed by a standard Fast Red detection protocol. Hematoxylin-counterstained slides were mounted with coverslips. Staining intensity was determined by a clinically certified pathologist who was blinded to all clinical data and antibodies used for IHC.

Chromatin Immunoprecipitation (ChIP)

ChIP was performed as previously described (Mersaoui et al., 2019).using the SimpleChip plus Chromatin IP Kit (CST; Magnetic beads 9005) according to the manufacturer's instruction. Briefly, formaldehyde cross-linked chromatin was prepared from $2x10^7$ B16.F10 melanoma cells, and the samples were immunoprecipitated with the corresponding antibodies (Dataset S3) overnight at 4°C and rabbit-IgG isotype control was used for mock precipitation to exclude any non-specific enrichment. The primers used for qPCR are listed in Dataset S3.

Strand-specific PCR for detection of sense and antisense ERV transcripts

The strand-specific PCR method was adapted from (Henke et al., 2015) (TASA-TD) and performed with the MultiScribe RT-PCR (Applied biosystems #4366596) with some modifications. Briefly, the gene and strand specific primers (GSP) were synthesized with an extra TAG sequence at the 5' end, which does not exist in the mouse genome (listed in Dataset S3). The first strand cDNA synthesis reaction was performed following these steps. 1 μg total RNA in 6 μl H2O was mixed with 1 μM TAG-GSP, 0.5 mM dNTP, 40 U RNase inhibitor, 100 U MultiScribe RT and 240 ng Actinomycin D (Sigma-Aldrich, #A9415) to a total volume of 20 μl; incubated at 42°C for 30 min and terminated at 85°C

Author Manuscript Author Manuscript Author Manuscript Author Manuscript

for 5 min. The resulting single sense or antisense cDNA/RNA hybrids were then treated with 2 U of recombinant RNase H (NEB #M0297S) to generate single strand cDNAs, followed by ethanol precipitation for cDNA purification. To amplify sense cDNA: a TAG primer and GSP sense (PCR) were used and to amplify antisense strand: a TAG primer and GSP antisense (PCR) were used. Sense and antisense specific PCRs for β-actin were used as an internal control (no antisense transcripts). The amplicons were visualized on 1.5% agarose gels.

dsRNA analysis by RT-qPCR

5 μg of total RNA extracted from B16.F10 cells was dissolved in 46 μl H2O and digested with 1U RNase A (Ambion #AM2270) under high salt condition: 3.5 μl NaCl (5 M stock) to a total volume of 50 μl and mixed well, followed by incubation for 30 min at 37°C. H_2O was used as mock. Then, 1 ml TRIzol was added to the mixture to terminate digestion, followed by RNA extraction. The transcript expression of selected retrotransposons was measured by RT-qPCR with GAPDH as an internal control. The dsRNA-fold enrichment was calculated as the ratio of retrotransposon/$GAPDH_{RNaseA}$/retrotransposon/$GAPDH_{mock}$.

dsRNA analysis by J2 immunoblotting

Total RNA extracted from B16.F10 cells was digested with mock (H_2O), RNaseIII (Thermo Fisher Scientific, #AM2290) according to the manufacturer's instructions, or with RNaseA (Ambion, #AM2270) under high salt condition (350 mM NaCl) as described previously (Sheng et al., 2018). Briefly, equal volumes of purified and treated RNA were dotted on Hybond N+ membrane (GE Healthcare, #RPN303B), dried and auto crosslinked in a UV machine (Bio-Rad GS Gene linker) using the following program: 125mJoule/cm^2 at 254 nM. The membrane was probed with J2 antibody at 4 °C overnight and ECL was applied for film development. For the loading control, membrane was stained for 30 min with methylene blue solution (0.3% w/v methylene blue + 30% v/v ethanol + 70% v/v H_2O).

Genomic DNA preparation, bisulfite conversion, and DNA methylation analysis for ERVs

gDNAs from B16.F10 samples were extracted using the DNA isolation kit (Qiagen, 69504). Bisulfite conversion was performed on 1 μg of gDNA using the EZ DNA Methylation Kit (Zymo Research, D5002). For methylation analysis, bisulfite-treated DNA was used as templates to amplify specific regions, and the PCR products were cloned into *pBluescript SK.* For each sample and each ERV, multiple clones were sequenced. The *MuERV-L* and *IAP* regions were amplified with one round of PCR, and the *MusD* and *Line-1* regions were amplified with two rounds of PCR (nested PCR) using specific primers (Dataset S3). All PCRs were performed using Taq Polymerase (Qiagen ID: 201445) as follows: 94°C for 3 min, 30 cycles of 94°C for 30 sec, 57°C (for *MuERV-L* and *IAP*) or 52°C (for *MusD* and *Line-1*) for 30 sec, and 72°C for 30 sec, followed by a final extension at 72°C for 10 min.

RNA sequencing and data analysis

RNA samples were purified using GenElute™ Mammalian Total RNA Miniprep Kit (RTN70, Sigma Aldrich). Total RNA was assessed for quality using an Agilent Tapestation 4200, and RNA sequencing libraries were generated using TruSeq Stranded mRNA Sample

Author Manuscript Author Manuscript Author Manuscript Author Manuscript

Prep Kit with TruSeq Unique Dual Indexes (Illumina, Hiseq4000, SR75 platform located at San Diego, CA; UCSD IGM Genomics Facility, La Jolla, CA). Samples were processed following manufacturer's instructions, starting with 50 ng of RNA and modifying RNA shear time to 5 min. Resulting libraries were multiplexed and sequenced with 100 base pair (bp) to a depth of approximately 30 million reads per sample. Samples were demultiplexed using bcl2fastq v2.20 Conversion Software (Illumina, San Diego, CA). Reads were mapped to the Genome Reference Consortium Mouse Build 38 patch release 6 (mm10/GRCm38.p6: primary assembly) (Frankish et al., 2019) using STAR v2.4 (Dobin et al., 2013).

Gene expression analysis:

Expression levels were estimated using HOMER V4.10 (Heinz et al., 2010). Afterwards, we employed DESeq2 (Love et al., 2014) to normalize the raw counts as rlog variance stabilized values, as well as to perform the differential expression analysis as previously described (Darbelli et al., 2017). For the volcano plot, genes were considered differentially expressed if they had an adjusted p value <0.05, a base mean higher than 100 and an absolute fold-change greater than 2. For the heat map, genes were considered differentially expressed if the samples with the highest and lowest expression are more than 2-fold different and one of the samples has 25 normalized reads (as in the HOMER tutorial).

Gene ontology:

GO term enrichment analysis of the differentially expressed genes was performed through one or more of the following: (1) STRING v11.0 (Szklarczyk et al., 2019), (2) GSEA V3.0 (Mootha et al., 2003), (3) Enrichr, (4) DAVID, (5) IPA. The list of differentially expressed genes was compared to a background of expressed genes, consisting of all expressed genes in the complete dataset (defined as all genes with the DESeq2 base mean higher than the first expression quartile). For differentially expressed genes, upregulated and downregulated genes with a base mean higher than 100 and an absolute fold-change greater than 2 were used for the analysis. Publicly available gene expression data was obtained from the CCLE (Cancer Cell Line Encyclopedia and Genomics of Drug Sensitivity in Cancer, 2015).and/or TCGA (Barretina et al., 2012).

Quantification and statistical analysis

All experiments were repeated at least two to three times, except as specified otherwise. All data are presented as mean ± standard error of the mean (SEM). Graph Pad Prism Version 6 was used to generate plots and additional statistical analysis. Significance of comparison between two groups was assessed either by the unpaired or paired Student-*t test*. The use of the specific tests as well as the number of animals and experimental replicates has been reported in each figure legend. Statistically significant results were defined as follows: * p <0.05; ** p <0.01; *** p <0.001; **** p <0.0001. Statistical analysis for RNA-seq was performed with DESseq2 for gene expression.

Supplementary Material

Refer to Web version on PubMed Central for supplementary material.

Author Manuscript Author Manuscript Author Manuscript Author Manuscript

Acknowledgements

We would like to thank Dr. Xiaoru Chen for the expert technical assistance with the tumor slicing and Christophe Goncalves for helpful discussions and Dr. David Fisher (Harvard Medical School, Boston, Massachusetts) for his generous donation of the MITF antibody. We thank Dr. Antonis Koromilas for stimulating discussions. This work was funded by grants from Canadian Institute of Health Research (FDN-154303 awarded to S.R.) and the US National Institutes of Health (R01AI1214030A1 awarded to T.C.). N.S. was a recipient of a McGill fellowship (The Rosenberg/ Unger/ Schwarzbard/ Kallchman Hematology Research Award) and now holds a fellowship award from the Fonds de la recherche en santé du Québec (FRQS).

References

Agolini E, Dentici ML, Bellacchio E, Alesi V, Radio FC, Torella A, Musacchia F, Tartaglia M, Dallapiccola B, Nigro V, et al. (2018). Expanding the clinical and molecular spectrum of PRMT7 mutations: 3 additional patients and review. Clin Genet 93, 675–681. [PubMed: 28902392]

Balachandran S, Roberts PC, Brown LE, Truong H, Pattnaik AK, Archer DR, and Barber GN (2000). Essential role for the dsRNA-dependent protein kinase PKR in innate immunity to viral infection. Immunity 13, 129–141. [PubMed: 10933401]

Barretina J, Caponigro G, Stransky N, Venkatesan K, Margolin AA, Kim S, Wilson CJ, Lehar J, Kryukov GV, Sonkin D, et al. (2012). The Cancer Cell Line Encyclopedia enables predictive modelling of anticancer drug sensitivity. Nature 483, 603–607. [PubMed: 22460905]

Bedford MT, and Clarke SG (2009). Protein arginine methylation in mammals: who, what, and why. Mol Cell 33, 1–13. [PubMed: 19150423]

Benit L, De Parseval N, Casella JF, Callebaut I, Cordonnier A, and Heidmann T (1997). Cloning of a new murine endogenous retrovirus, MuERV-L, with strong similarity to the human HERV-L element and with a gag coding sequence closely related to the Fv1 restriction gene. Journal Of Virology 71, 5652–5657. [PubMed: 9188643]

Berrens RV, Andrews S, Spensberger D, Santos F, Dean W, Gould P, Sharif J, Olova N, Chandra T, Koseki H, et al. (2017). An endosiRNA-Based Repression Mechanism Counteracts Transposon Activation during Global DNA Demethylation in Embryonic Stem Cells. Cell Stem Cell 21, 694–703 e697. [PubMed: 29100015]

Bhat P, Leggatt G, Waterhouse N, and Frazer IH (2017). Interferon-gamma derived from cytotoxic lymphocytes directly enhances their motility and cytotoxicity. Cell Death Dis 8, e2836. [PubMed: 28569770]

Bian K, and Murad F (2014). sGC-cGMP Signaling: Target for Anticancer Therapy. Advances In Experimental Medicine And Biology 814, 5–13. [PubMed: 25015797]

Bird L (2020). MDSC metabolite stuns T cells. Nat Rev Immunol 20, 352–353.

Blanc RS, Vogel G, Chen T, Crist C, and Richard S (2016). PRMT7 Preserves Satellite Cell Regenerative Capacity. Cell Rep 14, 1528–1539. [PubMed: 26854227]

Burgess HM, and Mohr I (2018). Defining the Role of Stress Granules in Innate Immune Suppression by the Herpes Simplex Virus 1 Endoribonuclease VHS. Journal Of Virology 92.

Canadas I, Thummalapalli R, Kim JW, Kitajima S, Jenkins RW, Christensen CL, Campisi M, Kuang Y, Zhang Y, Gjini E, et al. (2018). Tumor innate immunity primed by specific interferon-stimulated endogenous retroviruses. Nat Med 24, 1143–1150. [PubMed: 30038220]

Cancer Cell Line Encyclopedia, C., and Genomics of Drug Sensitivity in Cancer, C. (2015). Pharmacogenomic agreement between two cancer cell line data sets. Nature 528, 84–87. [PubMed: 26570998]

Chen DS, and Mellman I (2017). Elements of cancer immunity and the cancer-immune set point. Nature 541, 321–330. [PubMed: 28102259]

Chiappinelli KB, Strissel PL, Desrichard A, Li H, Henke C, Akman B, Hein A, Rote NS, Cope LM, Snyder A, et al. (2015). Inhibiting DNA Methylation Causes an Interferon Response in Cancer via dsRNA Including Endogenous Retroviruses. Cell 162, 974–986. [PubMed: 26317466]

Darbelli L, Choquet K, Richard S, and Kleinman CL (2017). Transcriptome profiling of mouse brains with qkI-deficient oligodendrocytes reveals major alternative splicing defects including self-splicing. Sci Rep 7, 7554. [PubMed: 28790308]

Author Manuscript Author Manuscript Author Manuscript Author Manuscript

DeWitte-Orr SJ, Mehta DR, Collins SE, Suthar MS, Gale M Jr., and Mossman KL (2009). Long double-stranded RNA induces an antiviral response independent of IFN regulatory factor 3, IFN-beta promoter stimulator 1, and IFN. J Immunol 183, 6545–6553. [PubMed: 19864603]

Dhar SS, Lee SH, Kan PY, Voigt P, Ma L, Shi X, Reinberg D, and Lee MG (2012). Transtail regulation of MLL4-catalyzed H3K4 methylation by H4R3 symmetric dimethylation is mediated by a tandem PHD of MLL4. Genes Dev 26, 2749–2762. [PubMed: 23249737]

Dhatchinamoorthy K, Colbert JD, and Rock KL (2021). Cancer Immune Evasion Through Loss of MHC Class I Antigen Presentation. Front Immunol 12, 636568. [PubMed: 33767702]

Dobin A, Davis CA, Schlesinger F, Drenkow J, Zaleski C, Jha S, Batut P, Chaisson M, and Gingeras TR (2013). STAR: ultrafast universal RNA-seq aligner. Bioinformatics 29, 15–21. [PubMed: 23104886]

Du J, Miller AJ, Widlund HR, Horstmann MA, Ramaswamy S, and Fisher DE (2003). MLANA/MART1 and SILV/PMEL17/GP100 are transcriptionally regulated by MITF in melanocytes and melanoma. Am J Pathol 163, 333–343. [PubMed: 12819038]

Esteve PO, Chin HG, Smallwood A, Feehery GR, Gangisetty O, Karpf AR, Carey MF, and Pradhan S (2006). Direct interaction between DNMT1 and G9a coordinates DNA and histone methylation during replication. Genes Dev 20, 3089–3103. [PubMed: 17085482]

Feng Y, Maity R, Whitelegge JP, Hadjikyriacou A, Li Z, Zurita-Lopez C, Al-Hadid Q, Clark AT, Bedford MT, Masson JY, et al. (2013a). Mammalian protein arginine methyltransferase 7 (PRMT7) specifically targets RXR sites in lysine- and arginine-rich regions. J Biol Chem 288, 37010–37025. [PubMed: 24247247]

Feng Y, Roy A, Masson E, Chen TT, Humphrey R, and Weber JS (2013b). Exposure-response relationships of the efficacy and safety of ipilimumab in patients with advanced melanoma. Clin Cancer Res 19, 3977–3986. [PubMed: 23741070]

Frankish A, Diekhans M, Ferreira AM, Johnson R, Jungreis I, Loveland J, Mudge JM, Sisu C, Wright J, Armstrong J, et al. (2019). GENCODE reference annotation for the human and mouse genomes. Nucleic Acids Res 47, D766–D773. [PubMed: 30357393]

Fujimura T, Ring S, Umansky V, Mahnke K, and Enk AH (2012). Regulatory T cells stimulate B7-H1 expression in myeloid-derived suppressor cells in ret melanomas. J Invest Dermatol 132, 1239–1246. [PubMed: 22189788]

Gantier MP, and Williams BR (2007). The response of mammalian cells to double-stranded RNA. Cytokine Growth Factor Rev 18, 363–371. [PubMed: 17698400]

Gao G, Zhang L, Villarreal OD, He W, Su D, Bedford E, Moh P, Shen J, Shi X, Bedford MT, et al. (2019). PRMT1 loss sensitizes cells to PRMT5 inhibition. Nucleic Acids Res 47, 5038–5048. [PubMed: 30916320]

Gao J, Shi LZ, Zhao H, Chen J, Xiong L, He Q, Chen T, Roszik J, Bernatchez C, Woodman SE, et al. (2016). Loss of IFN-gamma Pathway Genes in Tumor Cells as a Mechanism of Resistance to Anti-CTLA-4 Therapy. Cell 167, 397–404 e399. [PubMed: 27667683]

Griffin GK, Wu J, Iracheta-Vellve A, Patti JC, Hsu J, Davis T, Dele-Oni D, Du PP, Halawi AG, Ishizuka JJ, et al. (2021). Epigenetic silencing by SETDB1 suppresses tumour intrinsic immunogenicity. Nature 595, 309–314. [PubMed: 33953401]

Guccione E, and Richard S (2019). The regulation, functions and clinical relevance of arginine methylation. Nat Rev Mol Cell Biol 20, 642–657. [PubMed: 31350521]

Haghandish N, Baldwin RM, Morettin A, Dawit HT, Adhikary H, Masson JY, Mazroui R, Trinkle-Mulcahy L, and Cote J (2019). PRMT7 methylates eukaryotic translation initiation factor 2alpha and regulates its role in stress granule formation. Mol Biol Cell 30, 778–793. [PubMed: 30699057]

Heinz S, Benner C, Spann N, Bertolino E, Lin YC, Laslo P, Cheng JX, Murre C, Singh H, and Glass CK (2010). Simple combinations of lineage-determining transcription factors prime cis-regulatory elements required for macrophage and B cell identities. Mol Cell 38, 576–589. [PubMed: 20513432]

Henke C, Strissel PL, Schubert MT, Mitchell M, Stolt CC, Faschingbauer F, Beckmann MW, and Strick R (2015). Selective expression of sense and antisense transcripts of the sushiichi-related retrotransposon--derived family during mouse placentogenesis. Retrovirology 12, 9. [PubMed: 25888968]

Author Manuscript Author Manuscript Author Manuscript Author Manuscript

Higgs BW, Morehouse CA, Streicher K, Brohawn PZ, Pilataxi F, Gupta A, and Ranade K (2018). Interferon Gamma Messenger RNA Signature in Tumor Biopsies Predicts Outcomes in Patients with Non-Small Cell Lung Carcinoma or Urothelial Cancer Treated with Durvalumab. Clin Cancer Res 24, 3857–3866. [PubMed: 29716923]

Hoek KS, and Goding CR (2010). Cancer stem cells versus phenotype-switching in melanoma. Pigment Cell Melanoma Res 23, 746–759. [PubMed: 20726948]

Hoek KS, Schlegel NC, Brafford P, Sucker A, Ugurel S, Kumar R, Weber BL, Nathanson KL, Phillips DJ, Herlyn M, et al. (2006). Metastatic potential of melanomas defined by specific gene expression profiles with no BRAF signature. Pigment Cell Res 19, 290–302. [PubMed: 16827748]

Hogg SJ, Vervoort SJ, Deswal S, Ott CJ, Li J, Cluse LA, Beavis PA, Darcy PK, Martin BP, Spencer A, et al. (2017). BET-Bromodomain Inhibitors Engage the Host Immune System and Regulate Expression of the Immune Checkpoint Ligand PD-L1. Cell Rep 18, 2162–2174. [PubMed: 28249162]

Hou A, Hou K, Huang Q, Lei Y, and Chen W (2020). Targeting Myeloid-Derived Suppressor Cell, a Promising Strategy to Overcome Resistance to Immune Checkpoint Inhibitors. Front Immunol 11, 783. [PubMed: 32508809]

Hugo W, Zaretsky JM, Sun L, Song C, Moreno BH, Hu-Lieskovan S, Berent-Maoz B, Pang J, Chmielowski B, Cherry G, et al. (2016). Genomic and Transcriptomic Features of Response to Anti-PD-1 Therapy in Metastatic Melanoma. Cell 165, 35–44. [PubMed: 26997480]

Jain K, and Clarke SG (2019). PRMT7 as a unique member of the protein arginine methyltransferase family: A review. Arch Biochem Biophys 665, 36–45. [PubMed: 30802433]

Jain K, Jin CY, and Clarke SG (2017). Epigenetic control via allosteric regulation of mammalian protein arginine methyltransferases. Proc Natl Acad Sci U S A 114, 10101–10106. [PubMed: 28874563]

Jelinic P, Stehle JC, and Shaw P (2006). The testis-specific factor CTCFL cooperates with the protein methyltransferase PRMT7 in H19 imprinting control region methylation. PLoS Biol 4, e355. [PubMed: 17048991]

Jeong HJ, Lee HJ, Vuong TA, Choi KS, Choi D, Koo SH, Cho SC, Cho H, and Kang JS (2016). Prmt7 Deficiency Causes Reduced Skeletal Muscle Oxidative Metabolism and Age-Related Obesity. Diabetes 65, 1868–1882. [PubMed: 27207521]

Jeong HJ, Lee SJ, Lee HJ, Kim HB, Anh Vuong T, Cho H, Bae GU, and Kang JS (2020). Prmt7 promotes myoblast differentiation via methylation of p38MAPK on arginine residue 70. Cell Death Differ 27, 573–586. [PubMed: 31243342]

Kassiotis G, and Stoye JP (2016). Immune responses to endogenous retroelements: taking the bad with the good. Nat Rev Immunol 16, 207–219. [PubMed: 27026073]

Kato H, Takeuchi O, Sato S, Yoneyama M, Yamamoto M, Matsui K, Uematsu S, Jung A, Kawai T, Ishii KJ, et al. (2006). Differential roles of MDA5 and RIG-I helicases in the recognition of RNA viruses. Nature 441, 101–105. [PubMed: 16625202]

Kim H, Kim H, Feng Y, Li Y, Tamiya H, Tocci S, and Ronai ZA (2020). PRMT5 control of cGAS/STING and NLRC5 pathways defines melanoma response to antitumor immunity. Sci Transl Med 12.

Kim K, Skora AD, Li Z, Liu Q, Tam AJ, Blosser RL, Diaz LA Jr., Papadopoulos N, Kinzler KW, Vogelstein B, et al. (2014). Eradication of metastatic mouse cancers resistant to immune checkpoint blockade by suppression of myeloid-derived cells. Proc Natl Acad Sci U S A 111, 11774–11779. [PubMed: 25071169]

Kleffel S, Posch C, Barthel SR, Mueller H, Schlapbach C, Guenova E, Elco CP, Lee N, Juneja VR, Zhan Q, et al. (2015). Melanoma Cell-Intrinsic PD-1 Receptor Functions Promote Tumor Growth. Cell 162, 1242–1256. [PubMed: 26359984]

Kobayashi KS, and van den Elsen PJ (2012). NLRC5: a key regulator of MHC class I-dependent immune responses. Nat Rev Immunol 12, 813–820. [PubMed: 23175229]

Ku Y, Park JH, Cho R, Lee Y, Park HM, Kim M, Hur K, Byun SY, Liu J, Lee YS, et al. (2021). Noncanonical immune response to the inhibition of DNA methylation by Staufen1 via stabilization of endogenous retrovirus RNAs. Proc Natl Acad Sci U S A 118.

Author Manuscript Author Manuscript Author Manuscript Author Manuscript

Larkin J, Chiarion-Sileni V, Gonzalez R, Grob JJ, Cowey CL, Lao CD, Schadendorf D, Dummer R, Smylie M, Rutkowski P, et al. (2015). Combined Nivolumab and Ipilimumab or Monotherapy in Untreated Melanoma. N Engl J Med 373, 23–34. [PubMed: 26027431]

Larkin J, Chiarion-Sileni V, Gonzalez R, Grob JJ, Rutkowski P, Lao CD, Cowey CL, Schadendorf D, Wagstaff J, Dummer R, et al. (2019). Five-Year Survival with Combined Nivolumab and Ipilimumab in Advanced Melanoma. N Engl J Med 381, 1535–1546. [PubMed: 31562797]

Leem YE, Bae JH, Jeong HJ, and Kang JS (2019). PRMT7 deficiency enhances adipogenesis through modulation of C/EBP-beta. Biochem Biophys Res Commun 517, 484–490. [PubMed: 31371025]

Lehnertz B, Ueda Y, Derijck AA, Braunschweig U, Perez-Burgos L, Kubicek S, Chen T, Li E, Jenuwein T, and Peters AH (2003). Suv39h-mediated histone H3 lysine 9 methylation directs DNA methylation to major satellite repeats at pericentric heterochromatin. Curr Biol 13, 1192–1200. [PubMed: 12867029]

Li J, Byrne KT, Yan F, Yamazoe T, Chen Z, Baslan T, Richman LP, Lin JH, Sun YH, Rech AJ, et al. (2018). Tumor Cell-Intrinsic Factors Underlie Heterogeneity of Immune Cell Infiltration and Response to Immunotherapy. Immunity 49, 178–193 e177. [PubMed: 29958801]

Li T, Fan J, Wang B, Traugh N, Chen Q, Liu JS, Li B, and Liu XS (2017). TIMER: A Web Server for Comprehensive Analysis of Tumor-Infiltrating Immune Cells. Cancer Res 77, e108–e110. [PubMed: 29092952]

Li W, Xu H, Xiao T, Cong L, Love MI, Zhang F, Irizarry RA, Liu JS, Brown M, and Liu XS (2014). MAGeCK enables robust identification of essential genes from genome-scale CRISPR/Cas9 knockout screens. Genome Biol 15, 554. [PubMed: 25476604]

Love MI, Huber W, and Anders S (2014). Moderated estimation of fold change and dispersion for RNA-seq data with DESeq2. Genome Biol 15, 550. [PubMed: 25516281]

Lu C, Paschall AV, Shi H, Savage N, Waller JL, Sabbatini ME, Oberlies NH, Pearce C, and Liu K (2017). The MLL1-H3K4me3 Axis-Mediated PD-L1 Expression and Pancreatic Cancer Immune Evasion. J Natl Cancer Inst 109.

Ma D, Yang M, Wang Q, Sun C, Shi H, Jing W, Bi Y, Shen X, Ma X, Qin Z, et al. (2021). Arginine methyltransferase PRMT5 negatively regulates cGAS-mediated antiviral immune response. Sci Adv 7.

Maksakova IA, Mager DL, and Reiss D (2008). Keeping active endogenous retroviral-like elements in check: the epigenetic perspective. Cell Mol Life Sci 65, 3329–3347. [PubMed: 18818875]

Manguso RT, Pope HW, Zimmer MD, Brown FD, Yates KB, Miller BC, Collins NB, Bi K, LaFleur MW, Juneja VR, et al. (2017). In vivo CRISPR screening identifies Ptpn2 as a cancer immunotherapy target. Nature 547, 413–418. [PubMed: 28723893]

McCormick C, and Khaperskyy DA (2017). Translation inhibition and stress granules in the antiviral immune response. Nat Rev Immunol 17, 647–660. [PubMed: 28669985]

Medina-Echeverz J, Aranda F, and Berraondo P (2014). Myeloid-derived cells are key targets of tumor immunotherapy. Oncoimmunology 3, e28398. [PubMed: 25050208]

Mersaoui SY, Yu Z, Coulombe Y, Karam M, Busatto FF, Masson JY, and Richard S (2019). Arginine methylation of the DDX5 helicase RGG/RG motif by PRMT5 regulates resolution of RNA:DNA hybrids. EMBO J 38, e100986. [PubMed: 31267554]

Mootha VK, Lindgren CM, Eriksson KF, Subramanian A, Sihag S, Lehar J, Puigserver P, Carlsson E, Ridderstrale M, Laurila E, et al. (2003). PGC-1alpha-responsive genes involved in oxidative phosphorylation are coordinately downregulated in human diabetes. Nat Genet 34, 267–273. [PubMed: 12808457]

Ng CS, Jogi M, Yoo JS, Onomoto K, Koike S, Iwasaki T, Yoneyama M, Kato H, and Fujita T (2013). Encephalomyocarditis virus disrupts stress granules, the critical platform for triggering antiviral innate immune responses. Journal Of Virology 87, 9511–9522. [PubMed: 23785203]

Okamura K, and Lai EC (2008). Endogenous small interfering RNAs in animals. Nat Rev Mol Cell Biol 9, 673–678. [PubMed: 18719707]

Pardoll DM (2012). The blockade of immune checkpoints in cancer immunotherapy. Nat Rev Cancer 12, 252–264. [PubMed: 22437870]

Qin C, Wang Z, Shang J, Bekkari K, Liu R, Pacchione S, McNulty KA, Ng A, Barnum JE, and Storer RD (2010). Intracisternal A particle genes: Distribution in the mouse genome, active subtypes, and

Author Manuscript Author Manuscript Author Manuscript Author Manuscript

potential roles as species-specific mediators of susceptibility to cancer. Mol Carcinog 49, 54–67. [PubMed: 20025072]

Rehwinkel J, and Gack MU (2020). RIG-I-like receptors: their regulation and roles in RNA sensing. Nat Rev Immunol 20, 537–551. [PubMed: 32203325]

Riaz N, Havel JJ, Makarov V, Desrichard A, Urba WJ, Sims JS, Hodi FS, Martin-Algarra S, Mandal R, Sharfman WH, et al. (2017). Tumor and Microenvironment Evolution during Immunotherapy with Nivolumab. Cell 171, 934–949 e916. [PubMed: 29033130]

Roulois D, Loo Yau H, Singhania R, Wang Y, Danesh A, Shen SY, Han H, Liang G, Jones PA, Pugh TJ, et al. (2015). DNA-Demethylating Agents Target Colorectal Cancer Cells by Inducing Viral Mimicry by Endogenous Transcripts. Cell 162, 961–973. [PubMed: 26317465]

Salmaninejad A, Valilou SF, Shabgah AG, Aslani S, Alimardani M, Pasdar A, and Sahebkar A (2019). PD-1/PD-L1 pathway: Basic biology and role in cancer immunotherapy. J Cell Physiol 234, 16824–16837. [PubMed: 30784085]

Sheng W, LaFleur MW, Nguyen TH, Chen S, Chakravarthy A, Conway JR, Li Y, Chen H, Yang H, Hsu PH, et al. (2018). LSD1 Ablation Stimulates Anti-tumor Immunity and Enables Checkpoint Blockade. Cell 174, 549–563 e519. [PubMed: 29937226]

Shin DS, Zaretsky JM, Escuin-Ordinas H, Garcia-Diaz A, Hu-Lieskovan S, Kalbasi A, Grasso CS, Hugo W, Sandoval S, Torrejon DY, et al. (2017). Primary Resistance to PD-1 Blockade Mediated by JAK1/2 Mutations. Cancer Discov 7, 188–201. [PubMed: 27903500]

Su WY, Li JT, Cui Y, Hong J, Du W, Wang YC, Lin YW, Xiong H, Wang JL, Kong X, et al. (2012). Bidirectional regulation between WDR83 and its natural antisense transcript DHPS in gastric cancer. Cell Res 22, 1374–1389. [PubMed: 22491477]

Szewczyk MM, Ishikawa Y, Organ S, Sakai N, Li F, Halabelian L, Ackloo S, Couzens AL, Eram M, Dilworth D, et al. (2020). Pharmacological inhibition of PRMT7 links arginine monomethylation to the cellular stress response. Nat Commun 11, 2396. [PubMed: 32409666]

Szklarczyk D, Gable AL, Lyon D, Junge A, Wyder S, Huerta-Cepas J, Simonovic M, Doncheva NT, Morris JH, Bork P, et al. (2019). STRING v11: protein-protein association networks with increased coverage, supporting functional discovery in genome-wide experimental datasets. Nucleic Acids Res 47, D607–D613. [PubMed: 30476243]

Taube JM, Klein A, Brahmer JR, Xu H, Pan X, Kim JH, Chen L, Pardoll DM, Topalian SL, and Anders RA (2014). Association of PD-1, PD-1 ligands, and other features of the tumor immune microenvironment with response to anti-PD-1 therapy. Clin Cancer Res 20, 5064–5074. [PubMed: 24714771]

Topalian SL, Taube JM, Anders RA, and Pardoll DM (2016). Mechanism-driven biomarkers to guide immune checkpoint blockade in cancer therapy. Nat Rev Cancer 16, 275–287. [PubMed: 27079802]

Toyokawa G, Takada K, Tagawa T, Hamamoto R, Yamada Y, Shimokawa M, Oda Y, and Maehara Y (2019). A Positive Correlation Between the EZH2 and PD-L1 Expression in Resected Lung Adenocarcinomas. Ann Thorac Surg 107, 393–400. [PubMed: 30343006]

Vire E, Brenner C, Deplus R, Blanchon L, Fraga M, Didelot C, Morey L, Van Eynde A, Bernard D, Vanderwinden JM, et al. (2006). The Polycomb group protein EZH2 directly controls DNA methylation. Nature 439, 871–874. [PubMed: 16357870]

Wei SC, Anang NAS, Sharma R, Andrews MC, Reuben A, Levine JH, Cogdill AP, Mancuso JJ, Wargo JA, Pe'er D, et al. (2019). Combination anti-CTLA-4 plus anti-PD-1 checkpoint blockade utilizes cellular mechanisms partially distinct from monotherapies. Proc Natl Acad Sci U S A 116, 22699–22709. [PubMed: 31636208]

Wherry EJ, and Kurachi M (2015). Molecular and cellular insights into T cell exhaustion. Nat Rev Immunol 15, 486–499. [PubMed: 26205583]

Wiedemann GM, Aithal C, Kraechan A, Heise C, Cadilha BL, Zhang J, Duewell P, Ballotti R, Endres S, Bertolotto C, et al. (2019). Microphthalmia-Associated Transcription Factor (MITF) Regulates Immune Cell Migration into Melanoma. Transl Oncol 12, 350–360. [PubMed: 30502589]

Woods DM, Sodre AL, Villagra A, Sarnaik A, Sotomayor EM, and Weber J (2015). HDAC Inhibition Upregulates PD-1 Ligands in Melanoma and Augments Immunotherapy with PD-1 Blockade. Cancer Immunol Res 3, 1375–1385. [PubMed: 26297712]

Author Manuscript Author Manuscript Author Manuscript Author Manuscript

Wu Q, Schapira M, Arrowsmith CH, and Barsyte-Lovejoy D (2021). Protein arginine methylation: from enigmatic functions to therapeutic targeting. Nat Rev Drug Discov.

Xu J, and Richard S (2021). Cellular pathways influenced by protein arginine methylation: Implications for cancer. Mol Cell 81, 4357–4368. [PubMed: 34619091]

Yanai H, Chiba S, Hangai S, Kometani K, Inoue A, Kimura Y, Abe T, Kiyonari H, Nishio J, Taguchi-Atarashi N, et al. (2018). Revisiting the role of IRF3 in inflammation and immunity by conditional and specifically targeted gene ablation in mice. Proc Natl Acad Sci U S A 115, 5253–5258. [PubMed: 29712834]

Yang Y, and Bedford MT (2013). Protein arginine methyltransferases and cancer. Nat Rev Cancer 13, 37–50. [PubMed: 23235912]

Ying Z, Mei M, Zhang P, Liu C, He H, Gao F, and Bao S (2015). Histone Arginine Methylation by PRMT7 Controls Germinal Center Formation via Regulating Bcl6 Transcription. J Immunol 195, 1538–1547. [PubMed: 26179907]

Zhang H, Han C, Li T, Li N, and Cao X (2019). The methyltransferase PRMT6 attenuates antiviral innate immunity by blocking TBK1-IRF3 signaling. Cell Mol Immunol 16, 800–809. [PubMed: 29973649]

Zhang Q, Meng F, Chen S, Plouffe SW, Wu S, Liu S, Li X, Zhou R, Wang J, Zhao B, et al. (2017). Hippo signalling governs cytosolic nucleic acid sensing through YAP/TAZ-mediated TBK1 blockade. Nat Cell Biol 19, 362–374. [PubMed: 28346439]

Zhu J, Li X, Cai X, Zha H, Zhou Z, Sun X, Rong F, Tang J, Zhu C, Liu X, et al. (2021). Arginine monomethylation by PRMT7 controls MAVS-mediated antiviral innate immunity. Mol Cell 81, 3171–3186 e3178. [PubMed: 34171297]

Zhu J, Liu X, Cai X, Ouyang G, Fan S, Wang J, and Xiao W (2020a). Zebrafish prmt7 negatively regulates antiviral responses by suppressing the retinoic acid-inducible gene-I-like receptor signaling. FASEB J 34, 988–1000. [PubMed: 31914680]

Zhu J, Liu X, Cai X, Ouyang G, Zha H, Zhou Z, Liao Q, Wang J, and Xiao W (2020b). Zebrafish prmt3 negatively regulates antiviral responses. FASEB J 34, 10212–10227. [PubMed: 32643209]

Zurita-Lopez CI, Sandberg T, Kelly R, and Clarke SG (2012). Human protein arginine methyltransferase 7 (PRMT7) is a type III enzyme forming omega-NG-monomethylated arginine residues. J Biol Chem 287, 7859–7870. [PubMed: 22241471]

Author Manuscript Author Manuscript Author Manuscript Author Manuscript

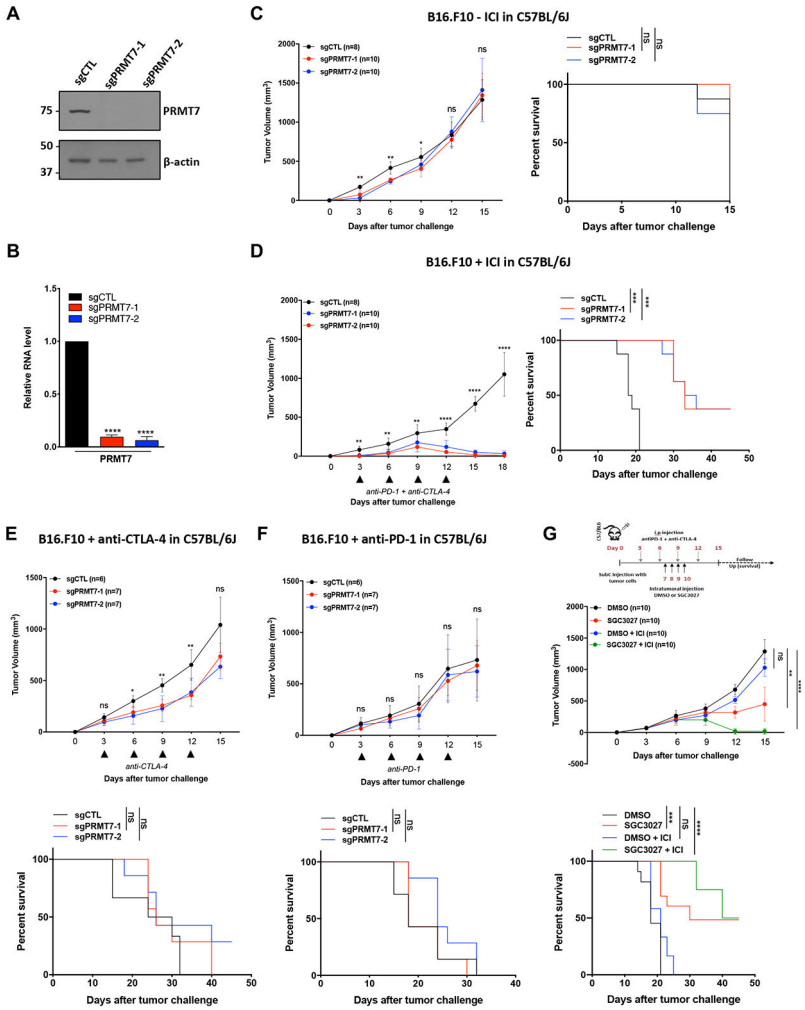

Figure 1: Deletion of PRMT7 sensitizes B16.F10 melanomas to ICIs.

(A) Western blot showing the expression of PRMT7 in sgCTL and sgPRMT7-1 and 2 targeted B16.F10 melanoma cells. β-actin is the loading control. Molecular mass markers are indicated in the left in kDa. One representative image out of three is shown.

(B) PRMT7 mRNA levels for clones in **(A)** measured by RT-qPCR. Data are mean ± SD. Data representative for four independent experiments. Statistical significance was calculated by unpaired student *t* test (**** $p < 0.0001$).

(C) Left panel: Tumor volume averaged for each group at each time point for sgCTL, sgPRMT7-1 and sgPRMT7-2 B16 cells injected into C57BL/6J mice without ICI treatment. Right panel: Kaplan-Meier survival curves were assessed at indicated time points. All groups reached the endpoint on the same day. Data are mean ± SEM; $n = 8$-10 mice per group.; p values were determined using multiple *t* test (* $p < 0.05$; ** $p < 0.01$; *ns*: non-significant).

(D) Left panel: Tumor volume averaged for each group at each time point for sgCTL, sgPRMT7-1 and sgPRMT7-2 B16 cells injected into C57BL/6J mice treated intraperitoneally with anti-CTLA-4 and anti-PD-1 (ICI) at day 3, 6, 9 and 12 (black triangles).

Author Manuscript Author Manuscript Author Manuscript Author Manuscript

Right panel: Kaplan-Meier survival curve was assessed at indicated time points. Data are mean ± SEM; *n* = 8-10 mice per group. Representative of two to three independent experiments is shown; *p* values were determined using multiple *t* test (***p* <0.01; ****p* <0.001; *****p* <0.0001).

(E-F) Upper panels: Tumor volume averaged for each group at each time point for sgCTL, sgPRMT7-1 and sgPRMT7-2 B16 cells injected into C57BL/6J mice treated intraperitoneally with anti-CTLA-4 alone **(E)** or anti-PD-1 **(F)** as performed in **(D)**.

Lower panels: Kaplan-Meier survival curve was assessed at indicated time points. Data are mean ± SEM; *n* = 6-7 mice per group. *p* values were determined using multiple *t* test (**p* <0.05; ***p* <0.01; *ns*: non-significant).

(G) Upper panel: Tumor volume averaged for each group at each time point for sgCTL cells injected into C57BL/6J mice treated or not with anti-CTLA-4 and anti-PD-1 (ICI) followed by intratumoral injection of DMSO or PRMT7 inhibitor (SGC3027) at indicated time points (day 7, 8, 9 and 10) as presented in the schema. One representative experiment is shown. Data are mean ± SEM; *n* = 10 mice per group. *p* values were determined using multiple *t* test (***p* <0.01; *****p* <0.0001; *ns*: non-significant).

Lower panels: Kaplan-Meier survival curve was assessed at indicated time points. Data are mean ± SEM; *n* = 10 mice per group. *p* values were determined using multiple *t* test (****p* <0.001; *****p* <0.0001; *ns*: non-significant).

Author Manuscript Author Manuscript Author Manuscript Author Manuscript

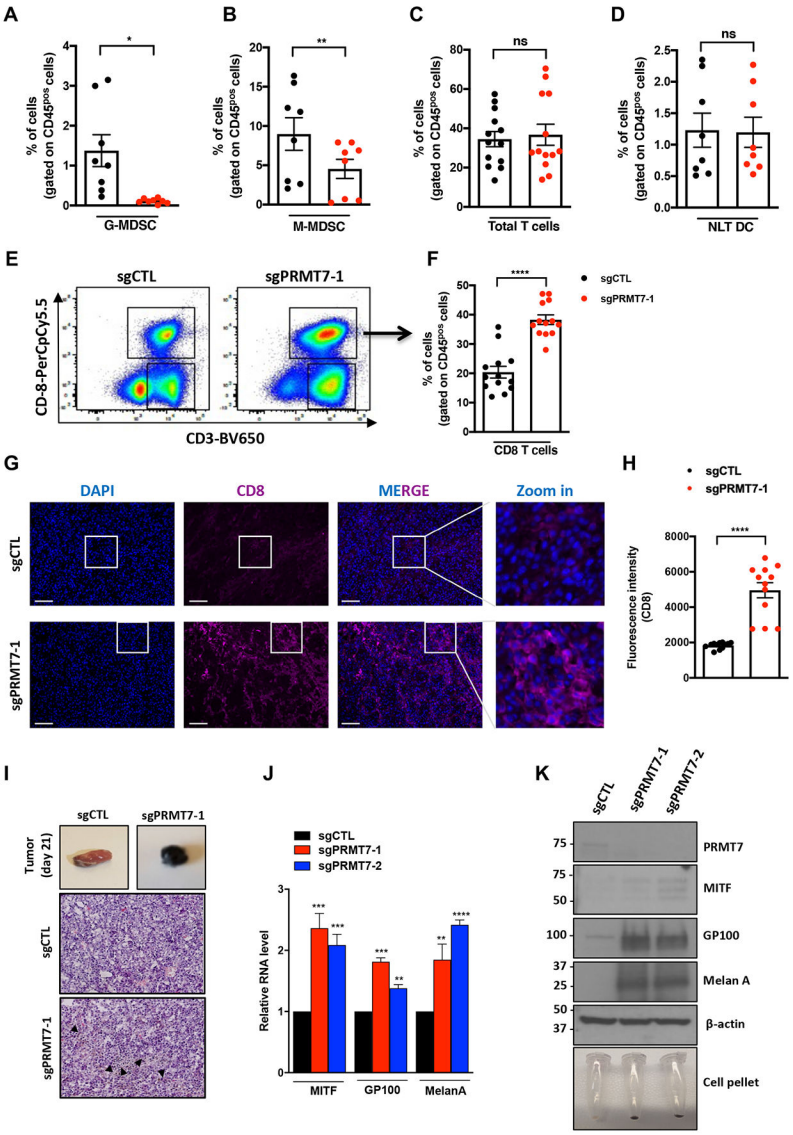

Figure 2: Deletion of PRMT7 in melanomas increases immune cell infiltration and increases melanocytic plasticity.

(A-D) Tumors were digested into a single cell suspension and their immune cell composition analyzed. Quantification of Myeloid-Derived Suppressor Cell (MDSC) populations such as Granulocytic MDSC (G-MDSC, F4/80^{neg}) **(A)**, Monocytic MDSC (M-MDSC, F4/80^{pos}) **(B)**, total T cells **(C)** and non-lymphatic dendritic cells (NLT DC) **(D)** in sgCTL (black) and sgPRMT7-1 (red) B16.F10 tumors. **(A-D)** The data represents the mean ± SD and is from two to three independent experiments with a minimum of 3 mice per group. Each dot represents one mouse. Statistical significance was calculated using paired student *t* test. (*p <0.05; **p <0.01; *ns*: non-significant).

(E) Representative flow cytometry plots using anti-CD45, anti-CD3 and anti-CD8 antibodies in sgCTL and sgPRMT7-1 B16.F10 tumors.

(F) Quantification graphs from (**E**) showing frequencies of double positive CD3^{pos}, CD8^{pos} cells (gated on CD45^{pos} cells) in sgCTL (black) and sgPRMT7-1 (red) B16.F10 tumors.

Author Manuscript Author Manuscript Author Manuscript Author Manuscript

Cells were gated as indicated and the relative percentage of cells shown; n=13 animals per group; data from three independent experiments. Statistical significance was calculated using paired student *t* test (****p <0.0001).

(G) Representative immunofluorescent images of sgCTL and sgPRMT7-1 tumor sections treated with anti-CTLA-4 and anti-PD-1 *in vivo* and stained with anti-CD8α antibody at 10x magnification. DAPI, 4',6-diamidino-2-phenylindole, was used to visualize nuclei by Zeiss confocal microscopy. A minimum of 3 biological replicates were used for each experiment.

(H) Immunofluorescence intensity of the CD8 staining done in (**G**) using ImageJ software. Bar graphs show fluorescence mean intensity ± SEM. Statistical significance was calculated using unpaired student *t* test (****p <0.0001).

(I) Representative pictures of subcutaneous sgCTL and sgPRMT7-1 derived-melanomas in C57BL/6J mice treated with anti-CTLA-4 and anti-PD-1 (day 21, top) and corresponding representative images of H&E-stained tumor sections (day 21, bottom). Black arrowheads indicate the pigmented areas.

(J) RT-qPCR analysis of *Mitf, Gp100* and *Melan-A* mRNA transcripts in sgCTL, sgPRMT7-1 and sgPRMT7-2 B16.F10 cells. Data are mean ± SD. Data representative for 3 independent experiments. Statistical significance was calculated by unpaired student *t* test (**p <0.01; ***p <0.001; ****p <0.0001).

(K) Western blot showing the expression of the indicated proteins (PRMT7, MITF, GP100 and Melan-A) in sgCTL, sgPRMT7-1 and sgPRMT7-2 B16.F10 melanoma cells. β-actin was used as the loading control. Molecular mass markers are indicated in the left in kDa. Data are representative of three independent experiments. Cell pellet representative images were shown (bottom; note the black pellet in sgPRMT7 clones).

Author Manuscript Author Manuscript Author Manuscript Author Manuscript

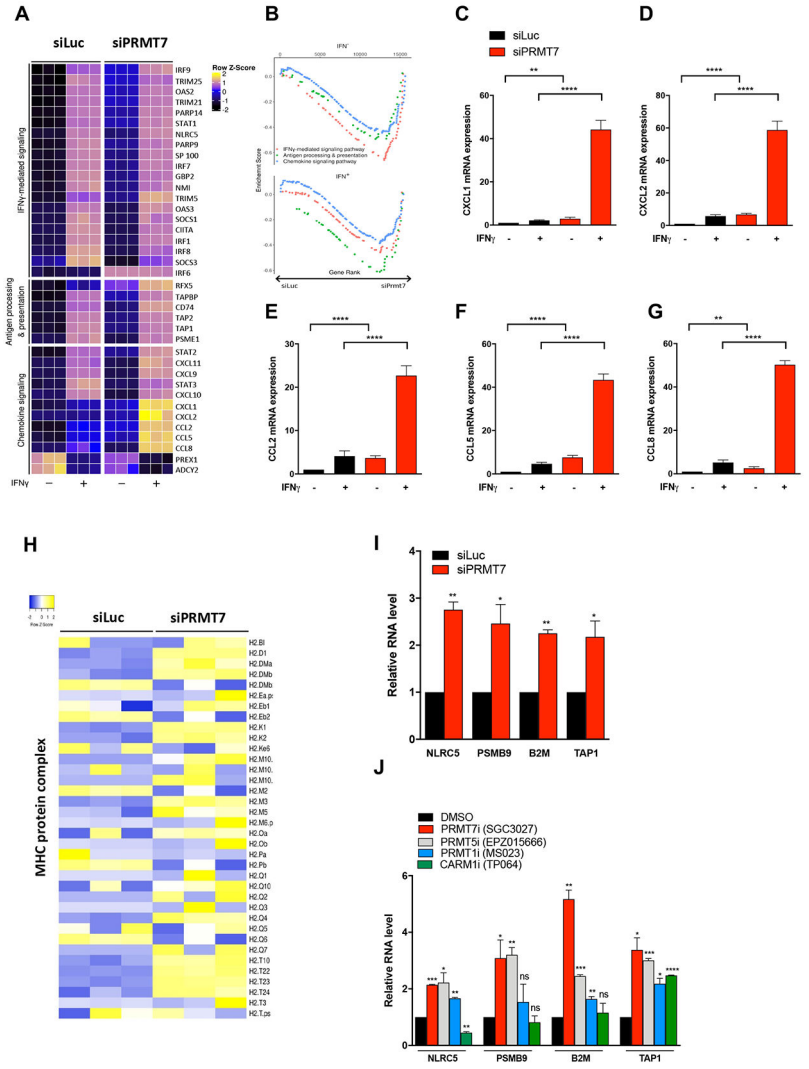

Figure 3: PRMT7 loss increases IFN pathway, antigen presentation and chemokine production

(A) siLuc and siPRMT7 B16.F10 cells (n=3 per group) were subjected to RNA-seq analysis. Heat map showing expression value (z-score based on cufflink count) of IFN genes, antigen processing and chemokine signaling genes with or without IFN-γ treatment (100 ng/ml) for 24h.

(B) Gene set enrichment analysis of IFN-γ signaling pathway antigen processing and presentation and chemokine signaling pathway in siLuc and siPRMT7 cells.

(C-G) RT-qPCR validation of genes identified from the RNA-seq dataset. Fold-change analysis using some selected genes: *Cxcl1* **(C)**, *Cxcl2* **(D)**, *Ccl2* **(E)**, *Ccl5* **(F)** and *Ccl8* **(G)** before and after IFN-γ treatment in siLuc (black) and siPRMT7 (red) B16.F10 cells. The fold-change in gene expression levels, before and after treatment, were calculated using the comparative cycle threshold (DDCT) method and values were normalized to Gapdh mRNA levels as an internal control. Triplicates were used per biological sample. Bar graphs represent the mean fold-change ± SD. Statistical significance was calculated by unpaired student *t* test (***p* <0.01; *****p* <0.0001).

Author Manuscript Author Manuscript Author Manuscript Author Manuscript

(H) Heat map showing expression value (z-score based on cufflink count) of all genes categorized in GO term 'MHC protein complex' in siLuc and siPRMT7 B16.F10 cells.
(I) RT-qPCR analysis of genes implicated in antigen presentation (*Nlrc5, Psmb9, B2m* and *Tap1*) in siLuc and siPRMT7 B16.F10 cells. Bar graphs represent the mean fold-change ± SD. Data are representative of three independent experiments. Statistical significance was calculated by unpaired student *t* test (**p* <0.1; ***p* <0.01).
(J) RT-qPCR analysis of same transcripts analyzed in **(I)** in B16.F10 cells treated with the indicated PRMT inhibitors for 48h (SGC3027: 10 μM; EPZ015666: 5 μM; MS023: 600 nM and TP064: 3 μM). Bar graphs represent the mean fold-change ± SD. Data are representative of three independent experiments. Statistical significance was calculated by unpaired student *t* test (**p* <0.1; ***p* <0.01; ****p* <0.001; *****p* <0.0001; *ns*: non-significant).

Author Manuscript Author Manuscript Author Manuscript Author Manuscript

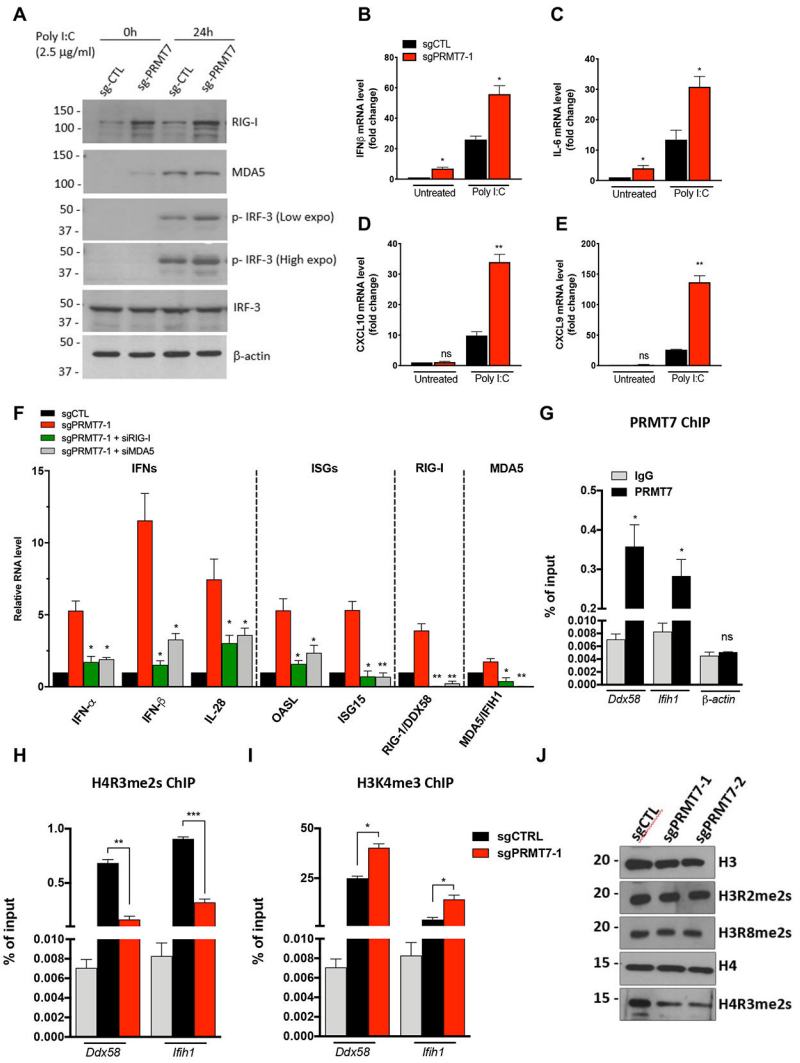

Figure 4: PRMT7 regulates *Ddx58* and *Ifih1* transcription levels by promoting H4R3me2s histone mark establishment at their promoters.

(A) Western blot analysis of RIG-I, MDA5, IRF-3 and p-IRF-3 expression in total cell lysates isolated from sgCTL and sgPRMT7-1 cells transfected or not with poly (I:C) at 2.5 µg/ml for 24 h. β-actin was used as the loading control. Data are representative of two independent experiments. The molecular mass markers are indicated in the left in kDa.

(B-E) RT-qPCR analysis of p-IRF-3 responsive genes (*Ifnβ, Il-6, Cxcl9* and *Cxcl10*) in sgCTL and sgPRMT7-1 cells transfected or not with poly (I:C) at 2.5 µg/ml for 24 h. Bar graphs represent the mean fold-change ± SD. Data are representative of two independent experiments. Statistical significance was calculated by unpaired student *t* test (**p* <0.1; ***p* <0.01; *ns*: non-significant).

(F) RT-qPCR analysis of *Ddx58, Ifih1*, some IFN genes (*Ifn-α., Ifn-β* and *Il-28*) and selected ISGs (*Oasl*, and *Isg15*) in sgCTL and sgPRMT7-1 cells transfected or not with siRIG-I or si-MDA5 for 72h. Bar graphs represent the mean fold-change ± SD. Data are representative of two independent experiments. Statistical significance was calculated by unpaired student *t* test (**p* <0.1; ***p* <0.01).

Author Manuscript Author Manuscript Author Manuscript Author Manuscript

(G) Chromatin was prepared from B16.F10 melanoma cells and analyzed by ChIP with a PRMT7-specific antibody (black bars). The immunoprecipitated chromatin fragments were then analyzed by qPCR with primers spanning *Ddx58* and *Ifih1* promoters. Results are normalized to input. *β-actin* served as a negative control.

(H-I) Analyses of distribution of H4R3me2s **(H)** and H3K4me3 **(I)** at the promoter regions of *Ddx58* and *Ifih1*. sgCTL and sgPRMT7-1 B16.F10 melanoma cells are represented in black and red bars, respectively. Chromatin was immunoprecipitated using anti-H4R3me2s and anti-H3K4me3. Anti-H3 and anti-H4 were used as controls for histone marks and IgG isotype was used for mock precipitation to exclude non-specific enrichment (grey bars). Subsequent qPCR was performed using promoter primer sets for *Ddx58* and *Ifih1*. Data were represented as percentage of input. Experiments were repeated two times. Asterisks denote significance in an unpaired *t* test (**p* <0.05; ***p* <0.01; ****p* <0.001; *ns*: non-significant), and error bars denote SD.

(J) Western blot analysis of acid-extracted histones using anti-H3, anti-H3R2me2s, anti-H3R8me2s, anti-H4 and anti-H4R3me2s in sgCTL, sgPRMT7-1 and sgPRMT7-2 B16.F10 melanoma cells. The data is representative of two independent experiments. Molecular mass markers are indicated in the left in kDa.

Author Manuscript Author Manuscript Author Manuscript Author Manuscript

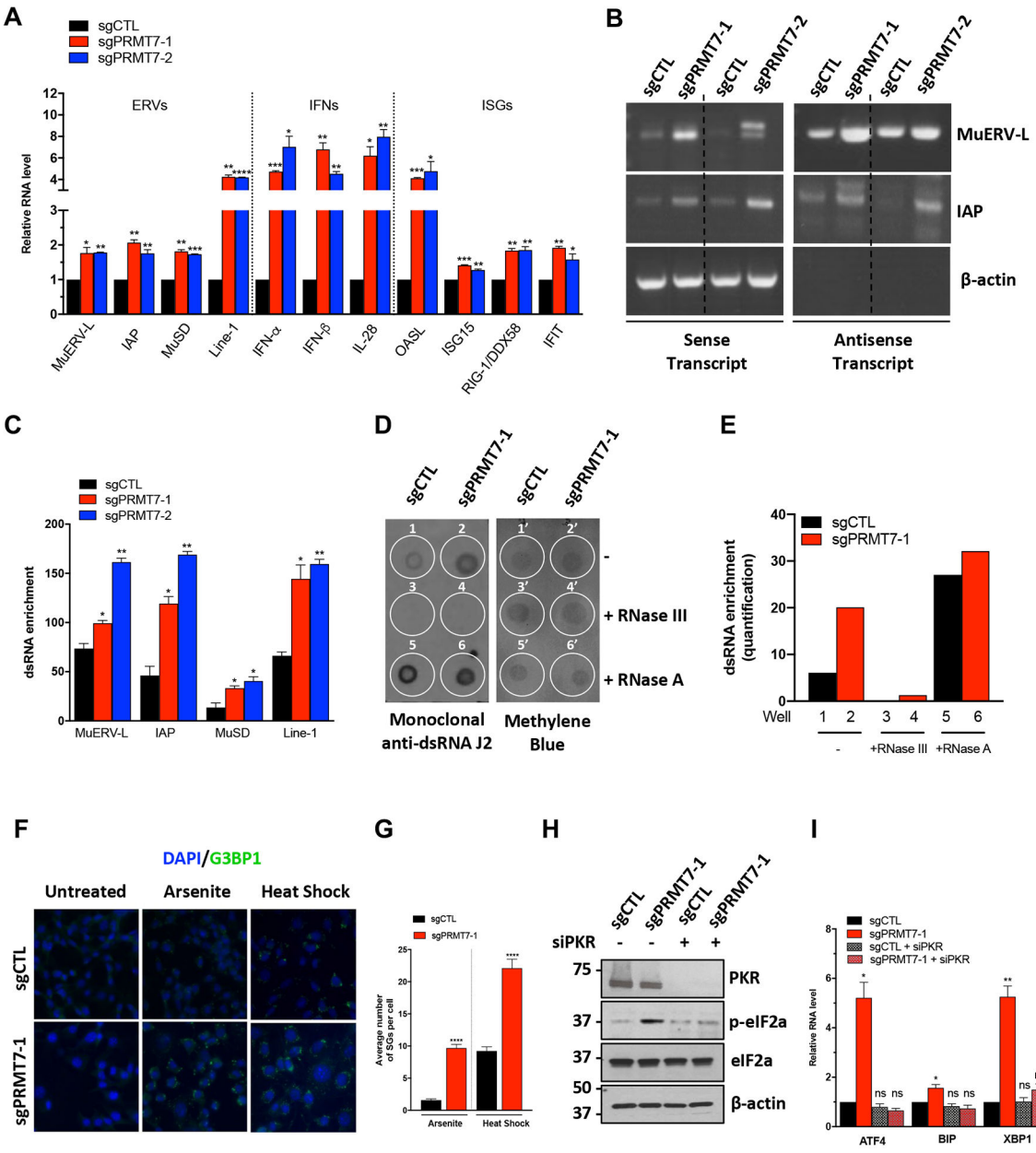

Figure 5: PRMT7 loss induces "viral mimicry" by regulating ERVs, dsRNA accumulation and stress granule (SG) formation.

(A) RT-qPCR analysis of selected retrotransposons, IFNs and ISGs transcripts in sgCTL, sgPRMT7-1 and sgPRMT7-2 B16 cells. Bar graphs represent the mean fold-change ± SD. Data are representative of three independent experiments. Statistical significance was calculated by unpaired student *t* test (**p* <0.1; ***p* <0.01; ****p* <0.001; *****p* <0.0001).

(B) The assessment of both sense and antisense transcripts of selected ERVs (*MuERV-L* and *IAP*) using strand-specific primers for RT-PCR (TASA-TD technique) in sgCTL, sgPRMT7-1 and sgPRMT7-2 B16 cells. *β-actin* was used as a negative control for antisense transcription. A representative experiment is shown of three independent experiments.

Author Manuscript Author Manuscript Author Manuscript Author Manuscript

(C) dsRNA enrichment of *MuERV-L IAP, MusD* and *Line-1* retrotransposons in sgCTL, sgPRMT7-1 and sgPRMT7-2 B16 cells by RT-qPCR analysis. RNase A treatment was used to digest ssRNAs and maintain the presence of dsRNAs.
(D) Total RNA extracted from sgCTL and sgPRMT7-1 B16 cells were treated with Mock, RNase III or RNase A (under high salt condition: 350 mM NaCl), dotted on Hybond N+ membrane and immunoblotted with the J2 antibody and visualized by methylene for loading control. Dots are denoted by numbers: 1, 3, 5 for sgCTL and 2, 4, 6 for sgPRMT7-1 cells nontreated (dots 1 and 2), treated with RNase III (dots 3 and 4) or RNase A (dots 5 and 6).
(E) Quantification of the J2 immunoblot presented in **(D)** using image J software and presented as a bar plot.
(F) sgCTL and sgPRMT7-1 B16 cells were incubated with 0.5 mM sodium arsenite for 1h or 45°C (heat shock) treatment for 30 min. Cells were then fixed with 4% PFA and immunostained using anti-G3BP1 antibodies. A representative IF image is shown 60x magnification. DAPI, 4',6-diamidino-2-phenylindole, was shown in blue as indicated.
(G) The average number of SGs per cell of the staining done in **(F)** was quantified using image J software and presented as a bar plot (n=60 to 70 cells per condition). Bar graphs show mean intensity ± SEM. Statistical significance was calculated by unpaired student t test (****p <0.0001).
(H) Western blot analysis of PKR, eIF2α and p- eIF2α expression in total cell lysates isolated from sgCTL and sgPRMT7-1 cells transfected with siCTL or siPKR for 72 h. β-actin was used as the loading control. Data are representative of two independent experiments. The molecular mass markers are indicated in the left in kDa.
(I) RT-qPCR analysis of p-eIF2α target genes (*Atf4, Bip, Xbp1*) in sgCTL, sgPRMT7-1 cells transfected or not with siPKR for 72 h. Bar graphs represent the mean fold-change ± SD. Data are representative of two independent experiments. Statistical significance was calculated by unpaired student *t* test (*p <0.1; **p <0.01; *ns*: non-significant).

Author Manuscript Author Manuscript Author Manuscript Author Manuscript

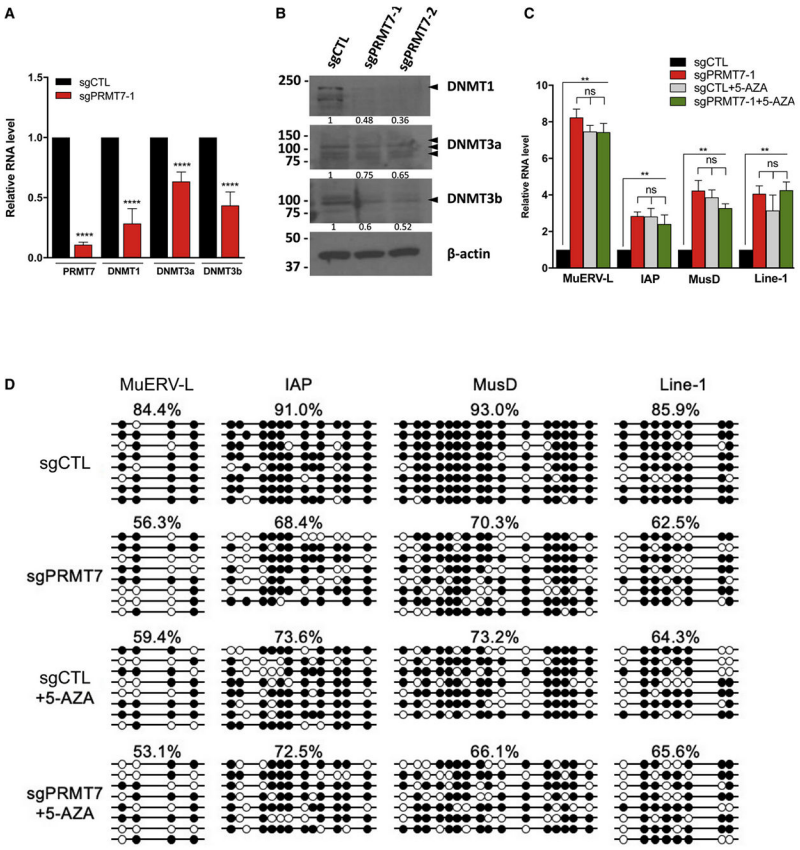

Figure 6: PRMT7-deficient B16 cells have decreased DNMT1, 3a, 3b expression and increased hypomethylation at ERV loci.

(A) RT-qPCR analysis of *DNMT* mRNAs (*Dnmt1, Dnmt3a* and *Dnmt3b*) in sgCTL, sgPRMT7 B16 melanoma cells. Bar graphs represent the mean fold-change ± SD. Data are representative of three independent experiments. Statistical significance was calculated by unpaired student *t* test (*****p* <0.0001).

(B) Immunoblot of DNMT proteins (DNMT1, DNMT3a and DNMT3b) in sgCTL, sgPRMT7-1 and sgPRMT7-2 B16 cells. β-actin was used as the loading control. A representative experiment is shown out of three independent experiments. The molecular mass markers are indicated in the left in kDa. The DNMT bands are shown with arrowheads. The value below each panel corresponds to the quantification by image J of DNMTs expression compared to sgCTL normalized to one.

(C) RT-qPCR analysis of *MuERV-L IAP, MusD* and *Line-1* retrotransposons in sgCTL, sgPRMT7-1 B16 cells treated or not with 5-Aza for 72 h. Bar graphs represent the mean fold-change ± SD. Data are representative of three independent experiments. Statistical significance was calculated by unpaired student *t* test (***p* <0.01; *ns*: non-significant).

(D) Bisulfite sequencing analysis of regions in the 5' LTRs of *MuERV-L, IAP* and *MusD* and the 5' UTR of *Line-1*, using genomic DNA isolated from sgCTL and sgPRMT7-1 B16.F10 cells treated or not with 5-Aza for 72 h. Each horizontal line represents one analyzed clone and at least 7 clones are presented for each sample. The black filled circles represent methylated CpG sites, while the white open circles represent unmethylated CpG sites. The percentages of methylated CpGs are shown at the top of each group of clones.

Author Manuscript Author Manuscript Author Manuscript Author Manuscript

Note that the numbers of CpG sites in *IAP* clones vary from 9 to 12 due to sequence variations.

Author Manuscript Author Manuscript Author Manuscript Author Manuscript

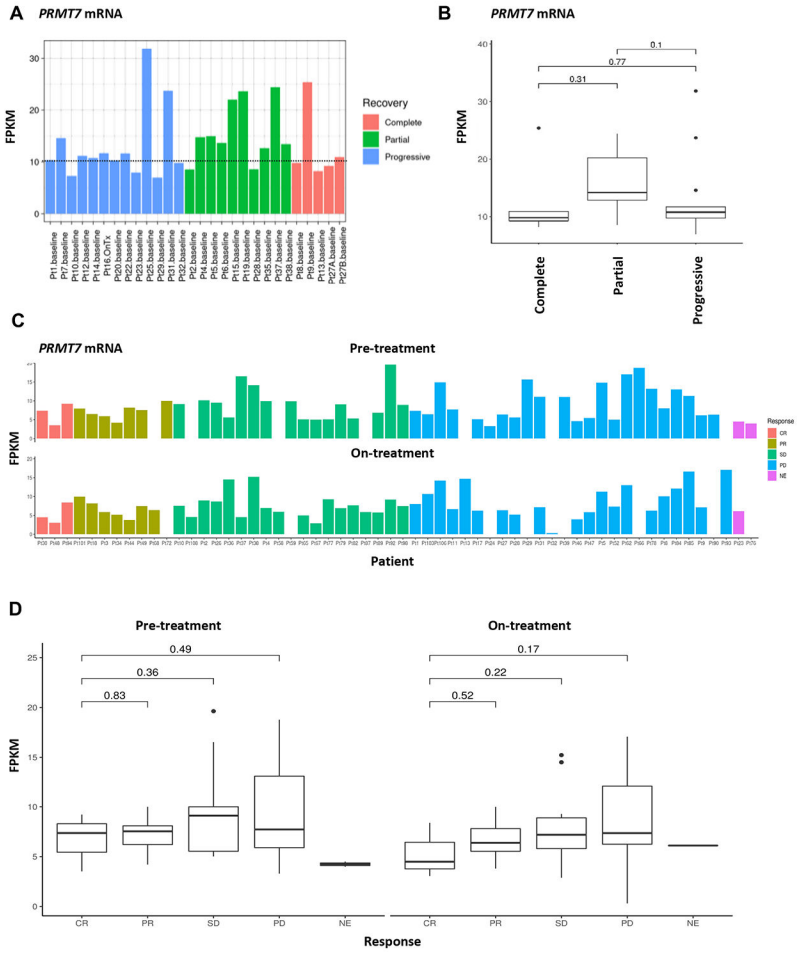

Figure 7: PRMT7 expression is inversely correlated with the response to ICI in human melanoma patients.

(A) Plot of FPKM gene expression values showing the correlation between PRMT7 mRNA expression in patients treated with ICI therapy. n=28 cases grouped according to whether they receive complete (pink; n=5), partial (green; n=10) or progressive recovery (blue; n=13). The FPKM values were obtained from the GEO accession GSE78220.

(B) Box plots showing the FPKM values for each case reported in (a). *p* values by Wilcoxon test are shown.

(C) Plot of the FPKM gene expression values for PRMT7 showing the correlation between PRMT7 in patients before (upper panel) and during (lower panel) Nivolumab treatment. n=58 cases grouped according to whether they showed a complete response (CR, orange; n=3), partial response (PR, olive; n=8) or stable disease (SD, green; n=19), progressive disease (PD, blue; n=26). 2 patients were non evaluable (NE, pink; n=2). The FPKM values were obtained from the GEO accession GSE91061.

(D) Box plots showing the FPKM values for each case reported in **(C)**. *p* values by Wilcoxon test are shown.

Author Manuscript
Author Manuscript
Author Manuscript
Author Manuscript

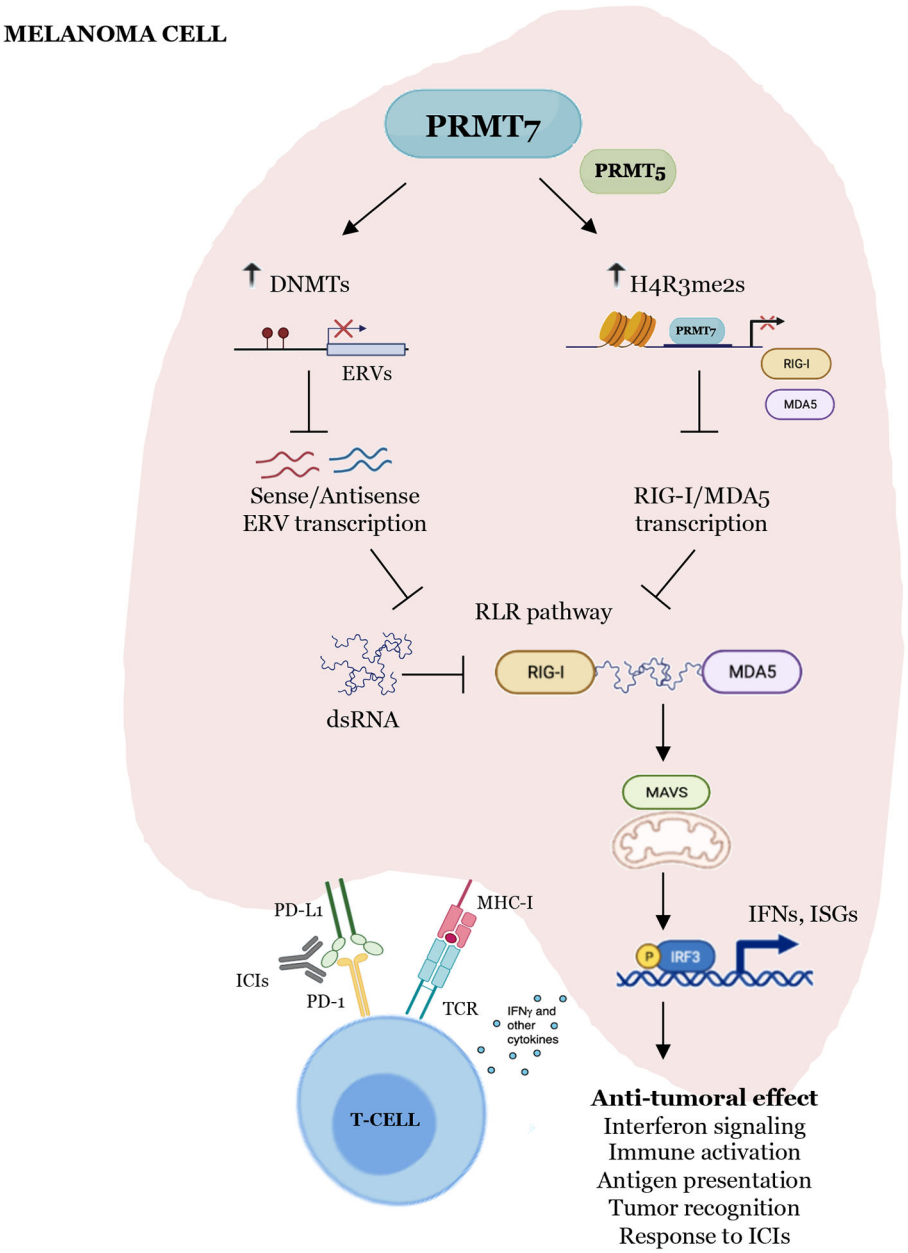

Figure 8: Proposed model for PRMT7 function in sensitizing melanoma to immunotherapy.

PRMT7 deletion or inhibition in melanoma enhances tumor immunogenicity and sensitivity to cancer immunotherapy by derepressing ERVs, activating RLR pathway, IFN response, antigen presentation and pro-inflammatory cytokines expression. This occurs through the decrease presence of H4R3me2s on *Ddx58 and Ifih1* promoters and influencing DNA methylation on selected ERVs.

Author Manuscript

Author Manuscript

Author Manuscript

Author Manuscript

Table 1:

Human melanoma correlative study

IHC staining towards CD3 and PRMT7 was established on nine human melanoma patient samples (FFPE tumor sections) treated with anti-PD-1 and carbotaxol. The level of CD3 and PRMT7 protein expression in the melanomas were scored and grouped according to whether they received clinical benefit from immunotherapy or not. 5 good responding tumors (GR: Good Responders) and 4 non-responding tumors (PR, Poor responders). The immune score was obtained from semi-quantitative prevalence of $CD3^+$ cells noted as absent (0), focal (1), moderate (2) or severe (3). For the PRMT7 staining, the score was noted as POS for a positive PRMT7 nuclear staining or as NEG for a negative PRMT7 nuclear staining (absence of PRMT7 expression: low or undetectable).

Patient ID	Response to ICI	PRMT7 Staining	Immune Score (CD3)
01-003	**PR**	POS	*1*
01-013	**PR**	NEG	x
01-022	**PR**	NEG	2
02-023	**PR**	POS	1
01-002	**GR**	NEG	2
01-004	**GR**	NEG	3
02-012	**GR**	POS	3
02-015	**GR**	NEG	3
02-025	**GR**	NEG	2